Engineering Reports

WILEY

Engineering Reports Open Access

RESEARCH ARTICLE OPEN ACCESS

Physical, Mechanical, and Volumetric Stability Properties of Mortar With Olive Waste Ash as Cement Substitute

Hassan Ghanem[1] | Safa Ghazzawi[1] | Jamal Khatib[1] | Adel Elkordi[1] | Mehmet Serkan Kırgız[2]

[1]Faculty of Engineering, Beirut Arab University, Beirut, Lebanon | [2]Faculty of Engineering, Istanbul Sabahattin Zaim University, Istanbul, Türkiye

Correspondence: Hassan Ghanem (h.ghanem@bau.edu.lb)

Received: 16 July 2025 | **Revised:** 17 October 2025 | **Accepted:** 3 November 2025

Keywords: expansion | mortar | olive waste ash | predictive model | shrinkage | sustainable construction material | volumetric stability

ABSTRACT

The environmental impact of Portland cement has led to the exploration of sustainable alternatives in construction materials. This study investigates the potential of olive waste ash (OWA), a byproduct of olive oil production, as a partial cement replacement in mortar. Five mixes were prepared with 0%–20% OWA, maintaining constant water-to-cement and sand-to-cement ratios (0.45 and 2:1, respectively). The mortars were evaluated for workability, ultrasonic pulse velocity (UPV), compressive and flexural strength, water absorption, and volumetric stability (chemical, autogenous, and drying shrinkage and expansion). Predictive models based on hyperbolic and capillary-diffusive functions were developed to assess compressive strength and moisture transport behavior over time. Results showed that 10% OWA yielded optimal performance, reducing chemical shrinkage, autogenous shrinkage, drying shrinkage, and expansion by 25%, 15%, 21%, and 24%, respectively. At this level, the compressive and flexural strengths were 23.5 and 2.8 MPa at 28 days, representing 24% and 15% reductions, respectively, relative to control. Model predictions correlated well with experimental data ($R^2 > 0.98$), confirming the reliability of the findings. This study demonstrates the potential of OWA as an eco-friendly cement substitute, improving volumetric stability while maintaining structural integrity in non-structural mortar applications.

1 | Introduction

Mortar is a widely used construction material employed in diverse applications, such as bedding and plastering of masonry walls, flexible pavement layers, and soil stabilization systems [1–6]. Despite its versatility, conventional mortar production relies heavily on Portland cement, a material known for its high carbon footprint. In response to the environmental concerns associated with cement manufacturing, there has been a growing interest in developing eco-friendly cementitious systems through the incorporation of supplementary cementitious materials (SCMs). One such promising SCM is olive waste ash (OWA), a byproduct obtained from the combustion of olive pomace—a residue from olive oil extraction [7–10]. Due to its pozzolanic properties and ecological benefits, OWA has attracted attention in the development of sustainable construction materials, including concrete, mortar, bricks, and geopolymers [8–12]. However, alongside sustainability, ensuring long-term durability and dimensional stability remains essential.

OWA, beyond its pozzolanic contribution, also represents an important pathway for waste valorization and emission reduction. The valorization of agricultural byproducts, such as OWA, reduces disposal burdens and offsets clinker consumption, contributing to carbon footprint reduction. Similar strategies have been applied to other waste-derived ashes. For instance, replacing natural sand with up to 20% municipal solid waste incineration bottom ash (MSW-IBA) in self-compacting

mortars reduced CO_2 emissions by about 5%–6%, production costs by 14%, and energy consumption by 5%, while still meeting engineering requirements for strength and workability, despite noticeable reductions in compressive and flexural strengths [13]. Incorporating IBA with Al_2O_3 micro-powder in high-strength mortars enhanced compressive strength by 3.8%–21.3% and flexural strength by 1.1%–9.8%, while reducing drying shrinkage by up to 28% and chloride migration by up to 39% [14]. In ultra-high-performance concretes, IBA combined with Al_2O_3 micro-powder improved compressive and flexural strengths by 12%–25%, reduced drying shrinkage by 20%, and achieved environmental benefits including a 7% CO_2 reduction, 11% energy savings, and 1% cost savings [15]. These findings highlight the dual role of such waste ashes in improving durability while advancing sustainable construction practices, supporting the rationale for exploring OWA in cement-based systems.

Mortar is particularly prone to volume changes resulting from various shrinkage mechanisms—chemical, autogenous, and drying—as well as expansion and creep-induced cracking [16, 17]. These deformations can compromise structural integrity if not adequately addressed.

Drying shrinkage, caused by water loss during the hardened phase, is a dominant factor affecting dimensional stability [18]. Studies show that partial cement replacement with materials such as high-calcium wood ash and fly ash can reduce drying shrinkage [19, 20]. In the context of OWA, its use in mortar and concrete has demonstrated potential in reducing long-term shrinkage and enhancing durability, especially at low replacement levels [1, 3, 10].

Autogenous shrinkage, or self-desiccation, results from internal water consumption during early hydration, without external moisture exchange [21]. It is influenced by several factors, including aggregate stiffness, sand-to-cement ratio, and surface roughness of the aggregates [22]. While fillers like clay and limestone fines have been shown to increase autogenous shrinkage [23, 24], the use of OWA has shown promise in mitigating it [25].

Chemical shrinkage occurs when the volume of hydration products is lower than that of the reactants (cement and water) [26]. It can be measured by dilatometry, pycnometry, or gravimetry [27]. Recent studies confirm that OWA, particularly at 10% replacement, can significantly reduce chemical shrinkage [25], with effects comparable to silica fume, fly ash, and slag [28]. Expansion, conversely, occurs when water absorption leads to matrix swelling. OWA incorporation has been reported to reduce expansion in cement pastes, further enhancing durability [12].

In addition to volume stability, the physical and mechanical performance of mortar containing OWA is also critical. Studies on OWA and other derived ashes have shown mixed results. For example, when OWA was combined with rice husk ash, synergistic pozzolanic reactions contributed to measurable strength gains [29, 30]. In contrast, stand-alone OWA replacements often resulted in strength losses, particularly at higher dosages, due to their relatively low reactivity [31, 32]. Some studies also suggest that the mode of replacement (sand vs. cement) plays a decisive role: sand replacement may provide a filler effect and improve strength [33], whereas cement replacement without complementary reactive SCMs often reduces performance [34]. These contrasting findings highlight that the effects of OWA are highly context dependent, underscoring the need for systematic evaluation.

In addition to agricultural waste valorization, sustainability in cementitious systems has also been pursued through recycled aggregate concrete (RAC) reinforced with fibers [35]. Advanced in situ 4D CT imaging techniques have enabled real-time visualization of crack propagation, fiber distribution, and interface optimization in carbonated RAC, while dynamic loading studies have provided constitutive models for toughness and energy dissipation [36–39]. Although distinct from the present focus on OWA-modified mortars, these works collectively emphasize the broader importance of linking material sustainability with structural performance.

2 | Research Significance

Despite previous studies on OWA in cementitious systems, there remains a gap regarding the comprehensive evaluation of volumetric stability in mortar across different replacement levels. Earlier research has mainly emphasized strength or durability indicators, with limited attention to shrinkage and expansion behaviors. This study advances the field by systematically assessing the effects of 0%–20% OWA replacement on flowability, UPV, compressive and flexural strength, water absorption, and four volumetric parameters: chemical shrinkage, autogenous shrinkage, drying shrinkage, and expansion. By combining experimental results with correlation analysis, the study clarifies the interrelationships between chemical shrinkage and other volumetric deformations, providing a more integrated understanding of dimensional stability in OWA-modified mortars. Furthermore, the incorporation of predictive modeling using hyperbolic and capillary-diffusive functions enables accurate simulation of compressive strength and moisture transport offering a reliable analytical complement to laboratory testing. Overall, this dual experimental–analytical framework establishes OWA not only as a sustainable alternative to cement but also as a material whose volumetric stability performance can be quantified and predicted with confidence.

3 | Experimental Work

3.1 | Materials and Mixture Proportions

A variety of materials were used in this investigation, including Ordinary Portland Cement (CN PA-L 42.5 Type I), natural sand, water, and OWA. The OWA was produced from olive pomace, a byproduct of the olive oil extraction process. The olive pomace was collected from an olive press in Zgharta, North Lebanon, and combusted in a closed boiler system under ambient air at a controlled temperature of 500°C for approximately 8 h. Temperature was regulated using a thermocouple-based PID controller, and the pomace was spread in shallow layers to ensure uniform heating and oxygen access. After natural cooling, the resulting ash was ground in a Los Angeles abrasion machine and sieved

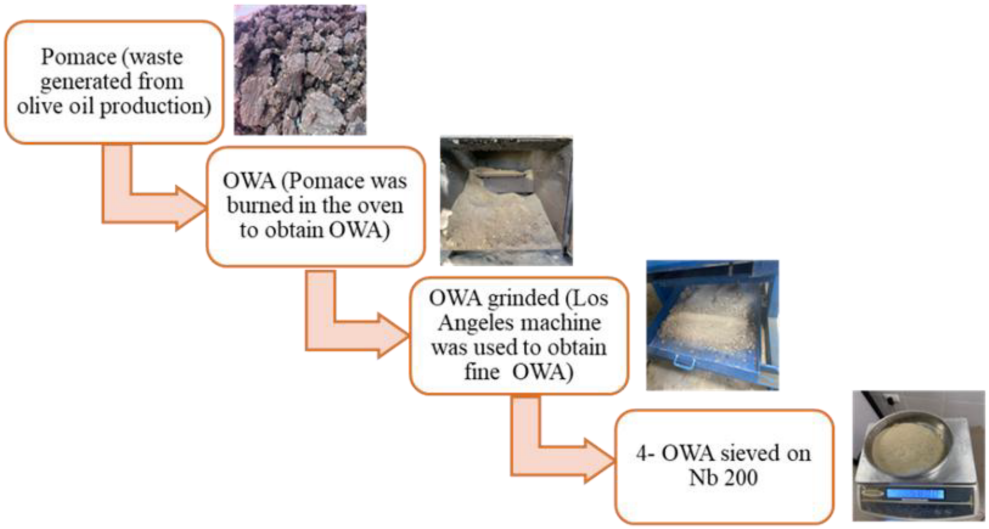

FIGURE 1 | OWA production procedure.

TABLE 1 | Particle size distribution of OWA and cement.

	Cumulative % passing	
Sieve (mm)	**OWA**	**Cement**
19	100	100
12.5	99	100
4.75	94	100
2	85	100
1.18	72	100
0.85	63	100
0.6	54	100
0.425	46	100
0.3	39	100
0.15	25	100
0.106	23	100
0.075	13	100
0.063	12	92
0.03	0	0

TABLE 2 | OWA and cement chemical composition (% by mass).

Oxide	OWA (%)	Cement (%)
SiO_2	24.73	18.53
Al_2O_3	3.41	3.93
Fe_2O_3	3.83	3.07
CaO	36.13	61.78
MgO	2.81	1.74
SO_3	0.03	2.92
K_2O	9.56	0.47
Na_2O	1.42	0.18
LOI	14.70	6.31
Other	3.38	1.09

through a No. 200 (75 μm) sieve to achieve uniform fineness. The degree of burnout was evaluated using a loss-on-ignition (LOI) test, which yielded 14.7%, indicating partial retention of carbonaceous matter—typical of low-temperature ashing aimed at preserving amorphous reactive phases rather than complete oxidation. Combustion gases were not analyzed; however, LOI served as a practical indicator of combustion efficiency. The produced OWA exhibited a bulk density of 950 kg/m^3 and a water absorption capacity of 28%. The complete preparation process is illustrated in Figure 1.

The particle size distribution and chemical composition of both OWA and cement are reported in Tables 1 and 2, respectively. The chemical composition of OWA indicates that the highest % corresponds to CaO (36.13%), followed by SiO_2 (24.73%). These higher proportions support the hypothesis that OWA can act as a pozzolanic material [25].

Five mortar mixtures with five percentages of 0%, 5%, 10%, 15%, and 20% of OWA replacing cement were produced. The water-to-cement ratio and the sand-to-cement ratio are maintained at 0.45 and 2, respectively, to ensure suitable workability while preserving sufficient strength or minimizing strength loss in the mortar specimens. Table 3 reveals the proportions and quantities of the mortar components. To assess workability, the flow table test is conducted as per ASTM C1437 guidelines [40]. This method offers key indicators on the consistency and flow features of the mixture by measuring the spread of the mixture during table drops.

3.2 | Testing Procedure and Specimen Preparation

For each test, three specimens are prepared and tested, and the average values are reported. The variability among replicates was within ±6% of the mean. The UPV and compressive strength of

TABLE 3 | Material breakdown and batch quantities of mortar mixes.

Quantities (kg/m^3)								
Mortar code	**Cement**	**OWA**	**W/C**	**S: C**	**Cement**	**OWA**	**Water**	**Sand**
M0%	1	0	0.45	2	657	0	296	1314
M5%	0.95	0.05	0.45	2	624	33	296	1248
M10%	0.9	0.1	0.45	2	591	66	296	1183
M15%	0.85	0.15	0.45	2	558	99	296	1117
M20%	0.8	0.2	0.45	2	526	131	296	1051

FIGURE 2 | (a) UPV test; (b) compressive strength test; and (c) flexural strength test.

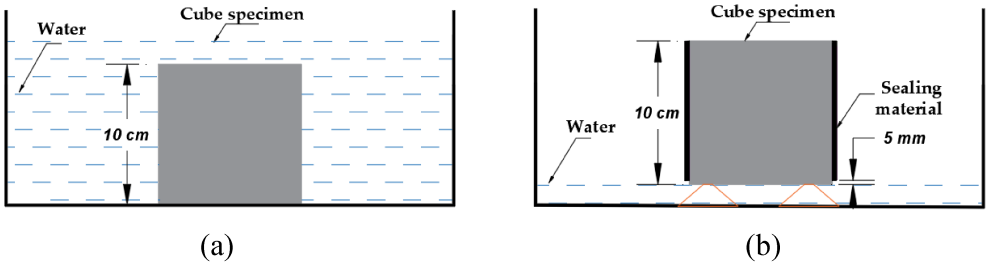

FIGURE 3 | Test setups for (a) TWA and (b) CWA.

mortars are tested on $50 \times 50 \times 50\,mm^3$ cubes adhering to ASTM C597 and ASTM C138 [41, 42] accordingly. For flexural strength testing, beams of $40 \times 40 \times 160\,mm^3$ are used according to ASTM C348 standards [43]. The corresponding tests are illustrated in Figure 2.

In the TWA evaluation, $100 \times 100 \times 100\,mm^3$ cubes are tested in accordance with ASTM C1585 guidelines [44]. After casting, demolding, and curing the samples until the specified testing dates, the samples are oven-dried for 48 h, as indicated in Figure 3a. Upon the removal of the cubes from the oven, the dry weight is then measured as (M_1). Afterward, the cubes are completely submerged in water for 5 min, and the initial weight is monitored as (M_2). This step is conducted again after 10, 20, 60, 120, and 450 min. The TWA percentage can be calculated as follows:

$$\text{TWA} = \frac{M_2 - M_1}{M_1} \times 100 \tag{1}$$

Concerning the CWA assessment, $100 \times 100 \times 100\,mm^3$ cubes are used following ASTM C1585 specifications [44]. The same methods of curing and drying applied for TWA evaluation are also followed in this test. To inhibit the water absorption, the samples are subsequently sealed on all sides, as depicted in Figure 3b. The dry weight of these samples is registered as M_1'. The cubes present a submerged weight of M_2' after 1 min of submersion. This process is then repeated after 3, 5, 10, 30, 60, 120, and 140 min, followed by measurements for the next 3 days. Based on the experimental findings, the equation of CWA is expressed as:

$$\text{CWA} = \frac{M_2' - M_1'}{A \cdot d} \tag{2}$$

where

$M_2' - M_1'$ = cumulative water absorption (kg)

A = surface area of the cube through which water penetrates (m^2)

d = density of water (kg/m^3)

The chemical shrinkage test is carried out in accordance with ASTM C1608, which measures the internal volume reduction in mortar due to cement hydration reactions [45]. The essential apparatus includes a 250 mL glass bottle, a 2 mL graduated pipette, a rubber stopper, and a spatula. In this procedure, 30 g of the mortar mix is placed into the bottle, resulting in a mixture depth of approximately 1.8 cm, as illustrated in Figure 4. Water is then gently added to saturate the contents up to the top of the bottle. The pipette is inserted through the stopper and positioned within the bottle, after which a drop of oil is placed on the pipette's surface to minimize evaporation. Chemical shrinkage is determined by monitoring the water level drop inside the pipette, with the initial measurement set as the zero reference point [46, 47]. Observations are recorded hourly during the first 24 h and subsequently every 2 days over a 90-day period. The shrinkage is then computed using the following formula:

$$\frac{\Delta V}{V} = 3\frac{\Delta L}{L} \tag{3}$$

where

ΔV = change in volume in the pipette (mL)

ΔL = change in length in the pipette (μm)

V = initial volume of the sample (mL)

L = initial length of the sample (m)

For the drying shrinkage test, molds of $25 \times 25 \times 300\,mm^3$ are tested according to ASTM C157 [48]. The data are recorded every 2 days for 90 days. Autogenous shrinkage is measured on sealed $25 \times 25 \times 300\,mm^3$ specimens in accordance with ASTM C192, using water-impermeable plastic films to prevent moisture escape [49]. The method of measuring the autogenous shrinkage is often similar to that used for measuring the drying shrinkage. Concerning the expansion test, the specimens are cast in $25 \times 25 \times 300^3$ mm molds. After demolding, each sample is completely submerged in water at a constant temperature of $20^{\circ}C \pm 1^{\circ}C$. The same procedure used to monitor drying shrinkage data is also applied for measuring expansion. The records are monitored with the length change comparator apparatus, as shown in Figure 5.

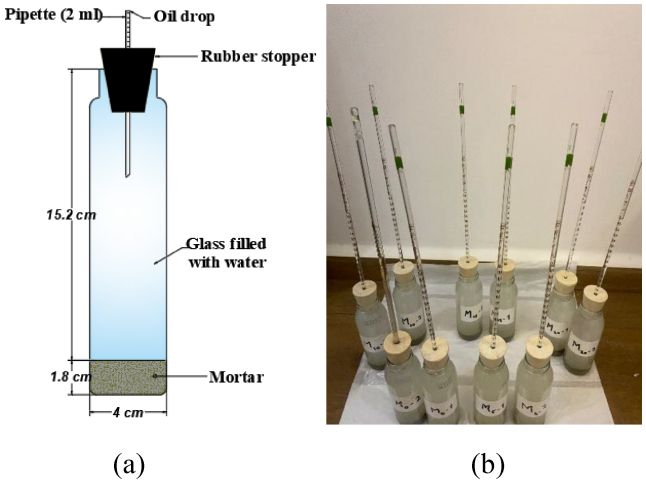

FIGURE 4 | (a) Chemical shrinkage evaluation setup and (b) chemical shrinkage samples.

FIGURE 5 | Length change comparator apparatus.

3.3 | Predictive Models Used in This Study

3.3.1 | Hyperbolic Model

To predict the compressive strength and length change characteristics, the hyperbolic model is proposed. This model is effective in determining the initial rate and ultimate value for each property, as indicated in Equation (4). This hyperbolic function is solved using MATLAB software.

$$P(t) = \frac{t}{\frac{1}{k} + \frac{t}{P_U}} \tag{4}$$

where $P(t)$ = property value at age t (length change or compressive strength) (μm/m or MPa); t = curing time (days); k = initial

rate parameter (μm/m/day or MPa/day); and P_U = ultimate property value (μm/m or MPa).

3.3.2 | Capillary-Diffusive Model

In investigating the durability of cement-based materials, it is critical to point out that water transport at an early age through capillarity is predominantly indicated by the sorptivity characteristic. Even though the sorptivity describes the near-surface absorption, another intrinsic parameter should be determined to evaluate the water flow through very tiny pores (deeper layers), which is caused by the diffusion mechanism [50, 51]. The diffusion action principally describes the water movement as well as the water permeability inside the mixture over longer periods [52]. A variety of factors contribute to absorption, either via capillarity or diffusion, including pore structure, curing regime, and preconditioning temperature [53–55]. More precisely, curing in water results in the opposite effect than curing in open air in a way to refine the pores, therefore augmenting the impermeability [53, 54]. Besides, a comparison between exposing the samples to high temperatures (100°C) and lower temperatures (50°C) clarifies that there is a significant improvement in sorptivity in the dried samples than in the partially dried ones. This behavior is related to greater capillary forces, which are applied to the pores to boost the passage of water [53, 54]. Whereas the diffusion is not impacted by the different temperatures [53, 54].

Water transport in mortar occurs in two distinct stages. In the initial stage, a linear relationship is observed between the mass of absorbed water per unit area (M/A) and the square root of immersion time ($t^{1/2}$), indicating rapid capillary ingress through the larger pore network. As water penetrates deeper into the specimen, the sorption rate gradually decreases due to the saturation of macropores; during this stage, the finer pores become the dominant pathways for moisture transport. Previous studies have also reported that the influence of gravitational forces on water absorption diminishes exponentially over time [53]. In general, the cumulative absorbed water, representing the combined effects of capillary and diffusive processes, can be expressed by Equation (5). To accurately describe this mechanism, Cuba proposed the capillary–diffusive function, which incorporates both sorptivity and diffusion parameters to model the absorption rate [53]. This approach is governed by two primary boundary conditions: (1) the assumption of a constant surface water concentration (C_0), and (2) the impermeability of the opposite surface of the specimen (length = 0.1 m). The resulting model, shown in Equation (6), defines the mass of absorbed water per unit area as a function of time and was solved using MATLAB software.

$$\frac{M}{A} = \text{capillary term} + \text{diffusion term} \tag{5}$$

$$\frac{M}{A} = C\rho\left(1 - \exp\frac{-St^{1/2}}{C\rho}\right) + C_0 L\left(1 - \frac{8}{\pi^2}\sum_{n=0}\frac{1}{(2n+1)^2}\exp\left[-Dt\frac{(2n+1)^2\pi^2}{4L^2}\right]\right) \tag{6}$$

where

M/A = Mass of water absorption per unit of area $\left(\text{kg/m}^2\right)$

C = Distance from the surface of concretewhere the first sorption is regulated by capillary pores

ρ = Water density $\left(\text{kg/m}^3\right)$

S = Sorptivity coefficient $\left(\text{kg/m}^2 \cdot s^{1/2}\right)$

t = Time (s)

C_0 = Water concentration constant $\left(\text{kg/m}^2\right)$

L = Depth of the specimen = 0.1 m

D = Coefficient of diffusion $\left(\text{m}^2/\text{s}\right)$

4 | Results and Discussion

4.1 | Workability

The workability of all mortar samples, measured using the flow table test according to ASTM C1437, is displayed in Figure 6.

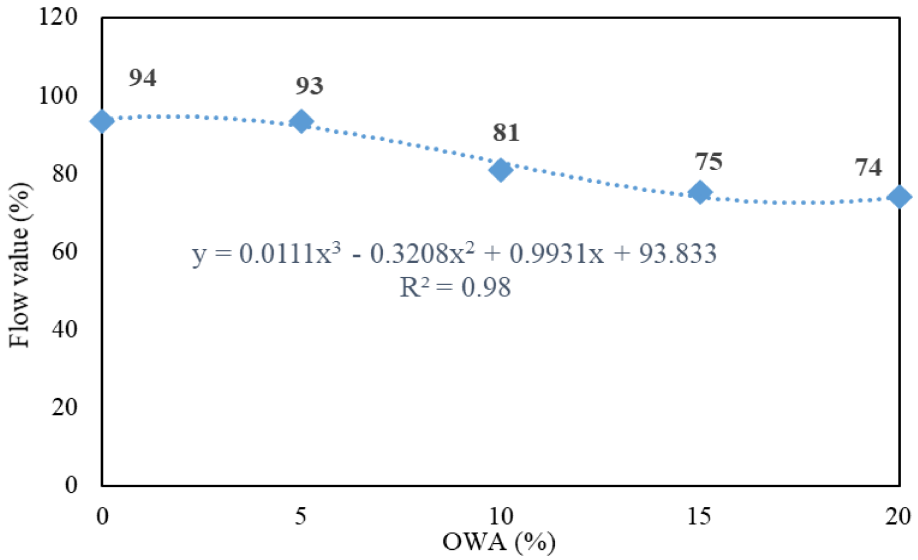

FIGURE 6 | Effect of OWA on the flow measurements of mortar specimens.

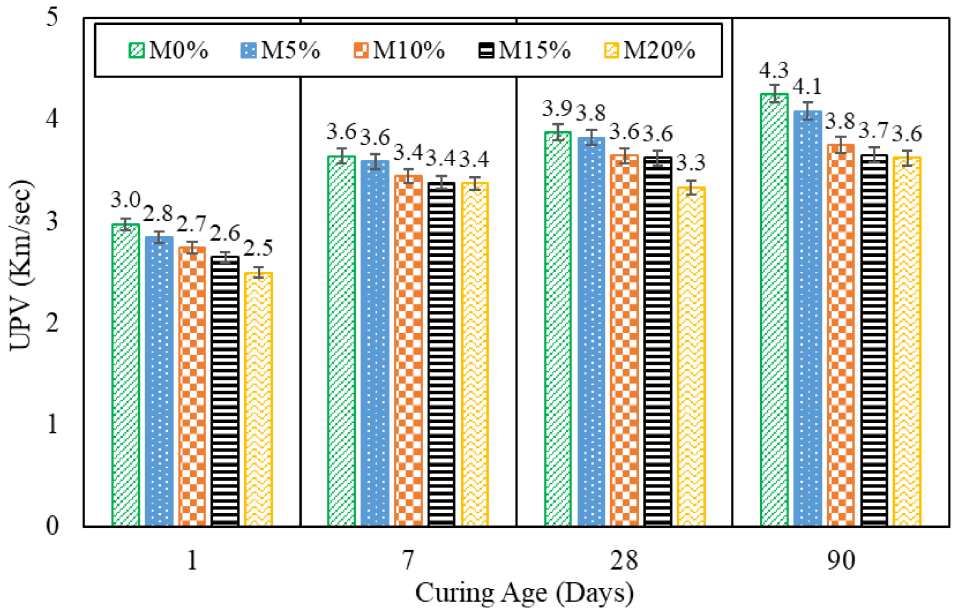

FIGURE 7 | UPV measurements.

In this method, flow is expressed as the percentage increase in spread diameter relative to the base diameter of the mold (110 mm), rather than in millimeters as used in slump flow tests for self-compacted concrete. As noted, the variation in flow values is relatively small between 0% and 5% OWA (1%). This minimal reduction can mostly be attributed to the restrained interference with available free water and particle packing. However, a drop in workability is observed through the reduction in the flow table values as the inclusion of OWA increases. For instance, the flow table varies between 81% and 74% for samples containing OWA varying from 10% to 20%, respectively, displaying decrease rates ranging from 13% to 21% relative to the control mortar. This significant drop is primarily due to the increased water demand and the morphology of OWA, including the irregular or round particle shape, and the water absorption of OWA [33]. Between 5% and 10% OWA, these physical properties become more impactful, contributing to augmenting the absorption of free water and limiting mixture packing. Nonetheless, beyond 15%, the decline in flow seems less pronounced, probably attributed to the fact that the mortar reaches a saturation point in terms of high levels of OWA exhibiting limited effect on water demand and particle interaction. The influence of the shape of ash particles on the workability behavior is stated in a previous study [56]. The relationship between OWA replacement level (x) and mortar flow value (F) was modeled using a cubic regression. The best-fit equation is obtained as $F(x) = 0.011x^3 - 0.321x^2 + 0.993x + 93.833$ with a coefficient of determination $R^2 = 0.98$. This strong correlation demonstrates the nonlinear reduction in workability—showing negligible change up to 5% OWA, followed by a sharp decline beyond 5%.

4.2 | Ultrasonic Pulse Velocity (UPV)

Figure 7 presents the UPV measurements for all samples at 1, 7, 28, and 90 days. The results show that UPV values decrease progressively as the OWA content increases. After 7 days of curing, the mixtures with 10%, 15%, and 20% OWA exhibit nearly constant UPV values, likely due to the dominance of early-age hydration and the limited pozzolanic activity of OWA at this stage. With longer curing, particularly at 28 and 90 days, the pozzolanic activity of OWA becomes more evident. At 90 days, the control mixture records the highest UPV (4.3 km/s), while the values for mortars containing 5%, 10%, 15%, and 20% OWA decline to 4.1, 3.8, 3.7, and 3.6 km/s, respectively. These represent reductions of approximately 4%, 12%, 14%, and 15% compared to the control. The decrease in UPV is primarily attributed to the dilution of cement by OWA, which reduces hydration products, and the higher porosity of OWA mixes that impedes ultrasonic wave propagation [57].

4.3 | Compressive and Flexural Strength

Figure 8 depicts the compressive strength results for all mixtures measured at 1, 7, 28, and 90 days. As seen, introducing OWA into the mortar results in a progressive decline in compressive strength compared to the OWA-free mortar. At 28 days, the compressive strength values for 0%, 5%, 10%, 15%, and 20% OWA content are 31.1, 28.3, 23.5, 18.2, and 15.4 MPa, respectively, indicating drops of approximately 9%, 24%, 41%, and 50%. Such reductions may be assigned to the reduced cement amount in the matrix, which leads to the loss of hydration products and impairs the overall strength of the matrix [58]. Additionally, less effective packing between the cement pastes and aggregates, especially within the interfacial transition zone (ITZ), can be a reasonable factor contributing to the observed strength loss [29]. Beyond these factors, the strength reduction can also be explained in terms of dilution and latent reactivity effects. The dilution effect arises because replacing cement with less reactive OWA lowers the clinker content and thus the immediate formation of hydration products, particularly calcium silicate hydrate (C-S-H). However, the presence of amorphous silica and alkali oxides in OWA suggests a latent pozzolanic potential that may become more

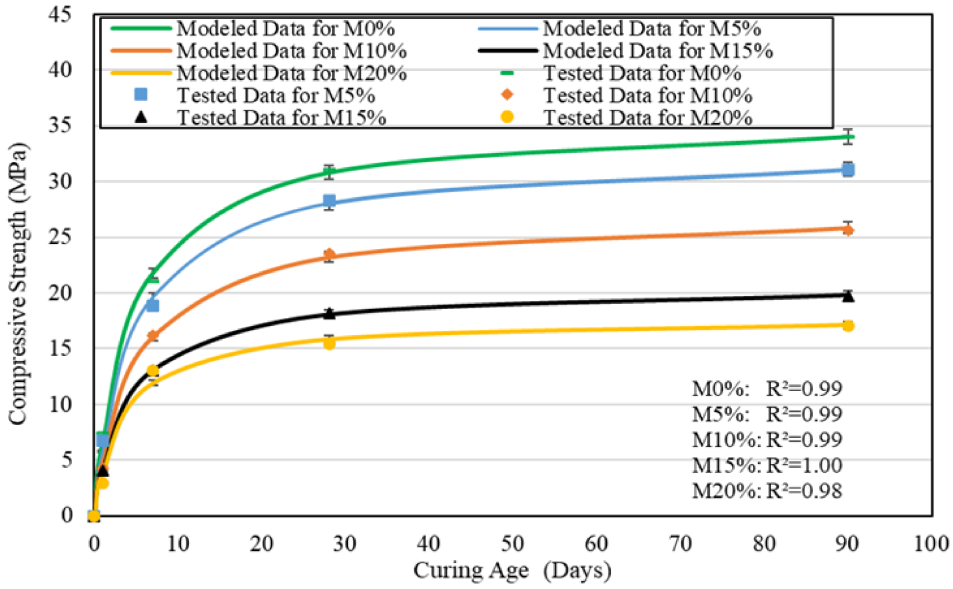

FIGURE 8 | Tested and modeled compressive strength.

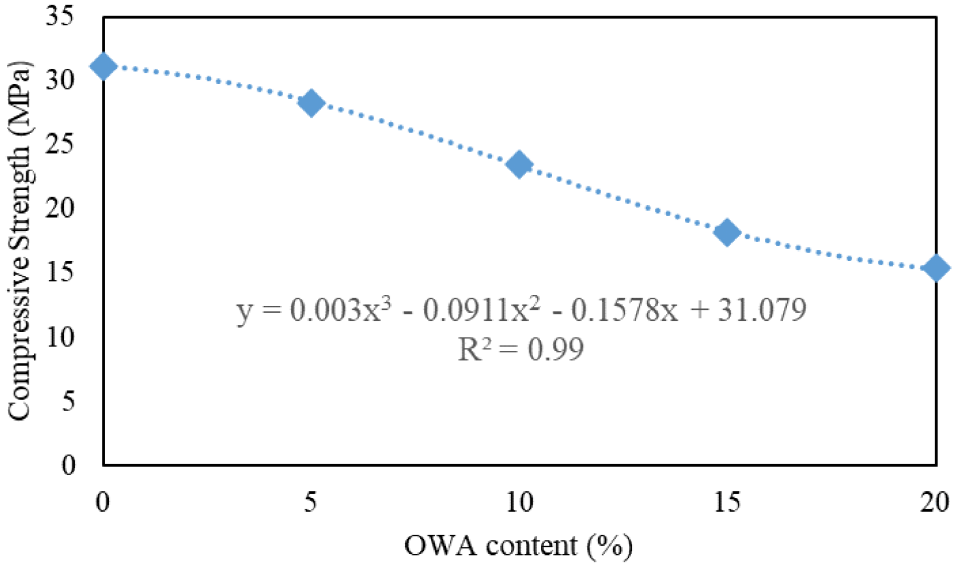

FIGURE 9 | Effect of OWA on the compressive strength of mortar specimens.

pronounced at later curing ages, partially mitigating early strength losses [59].

Contextualizing the obtained results, date palm ash (DPA) demonstrated a lower 28-day compressive strength performance, indicating a remarkable drop of 20% at a 20% substitution level [60]. In the case of cement replacement with corncob ash, the compressive strength fluctuated after 28 days of curing [61]. Replacing up to 10% of cement with corncob ash enhanced the strength by 25%, whereas exceeding this threshold led to a decline of roughly 15% relative to the reference concrete [61]. The contribution of wood ash retrieved from the combustion of a combination of wood-based residues to cement-based materials as a substitute for ordinary cement was also examined [62]. As a result, beyond the 10% threshold, there is a considerable enhancement in the 28-day compressive strength of concrete mixtures by 9%, attributable to the potential filler action of wood ash, along with its cementitious characteristics [62].

The relationship between OWA replacement level and mortar compressive strength is modeled through a cubic regression, as illustrated in Figure 9. The best-fit equation is $F(x) = 0.003x^3 - 0.091x^2 - 0.158x + 31.079$ with a high coefficient of determination $R^2 = 0.99$. This robust association confirms the nonlinear drop in compressive strength, with the lowest influence observed at up to 5% OWA, followed by a continuous decline beyond this level.

It is worth mentioning that the strength activity index (SAI) is a key parameter to evaluate the contribution of a resource to the development of absolute strength of cement-based materials. In this study, the SAI is calculated by dividing the compressive

strength of the OWA-based mortar by that of the control mortar at 28 days. For 5% and 10% OWA content, the SAI values stand at 91% and 75.5%, respectively, meeting the ASTM C618-00 specifications [63]. As a result, OWA can maintain its strength, primarily due to its pozzolanic reactivity with calcium hydroxide released during cement hydration, forming additional calcium silicate hydroxide (C-S-H) gel that enhances both strength and durability.

The hyperbolic model used to validate the compressive strength over time yields strong agreement with the experimental data, which is supported by the high coefficient of determination ($R^2 = 0.99$). This verifies the accuracy of the suggested model in describing the compressive strength behavior. Moreover, the evolution of both ultimate compressive strength (UCS) and initial rate of compressive strength (IRCS) is illustrated in Figure 10. As inferred, all samples follow a trend consistent with the compressive strength, showing that UCS and IRCS behave identically. For instance, the reference sample witnesses the highest UCS and IRCS values, peaking at 35.7 MPa and 8 MPa/day, respectively. As OWA content increases, both characteristics progressively decline—UCS decreases from 32.7 to 17.8 MPa and IRCS drops from 7 to 5 MPa/day—displaying reductions of roughly 8%–50% for UCS and 12%–35% for IRCS. The decrease in UCS may be explained by the formation of voids, which compromises long-term strength development [29]. Meanwhile, the decline in IRCS is attributed to the fact that OWA retards the early-age hydration process [25].

Furthermore, the flexural strength findings, monitored at 1, 7, 28, and 90 days, are displayed in Figure 11. As observed, the flexural strength gradually decreases as OWA levels increase. More precisely, the mixtures with 0%, 5%, 10%, 15%, and 20% OWA

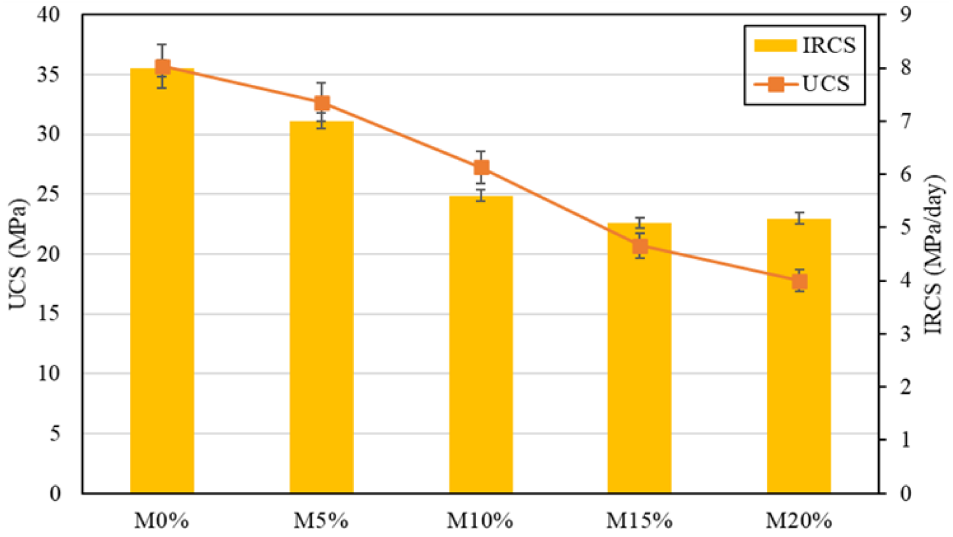

FIGURE 10 | Model outputs for compressive strength measurements (IRCS and UCS).

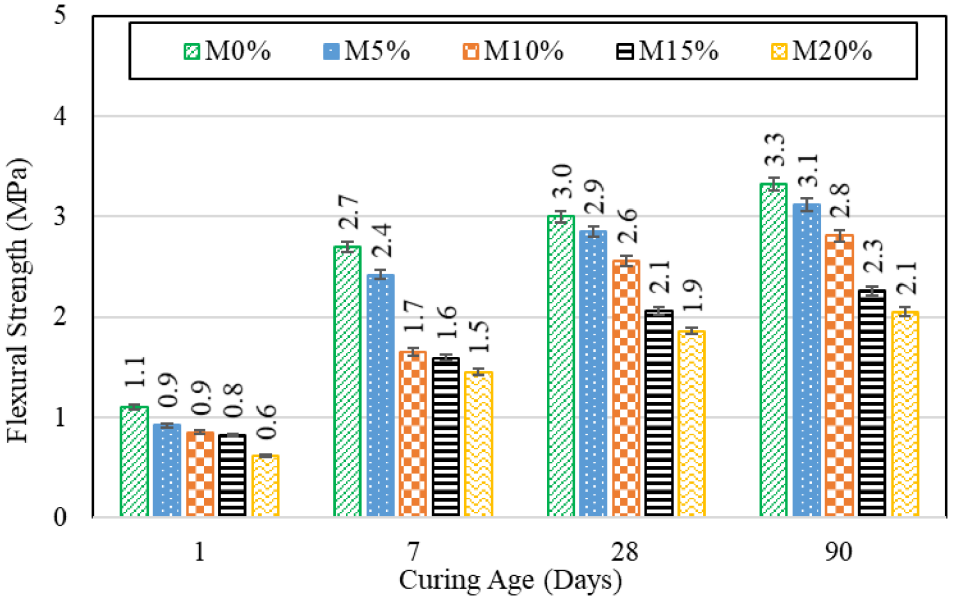

FIGURE 11 | Flexural strength measurements.

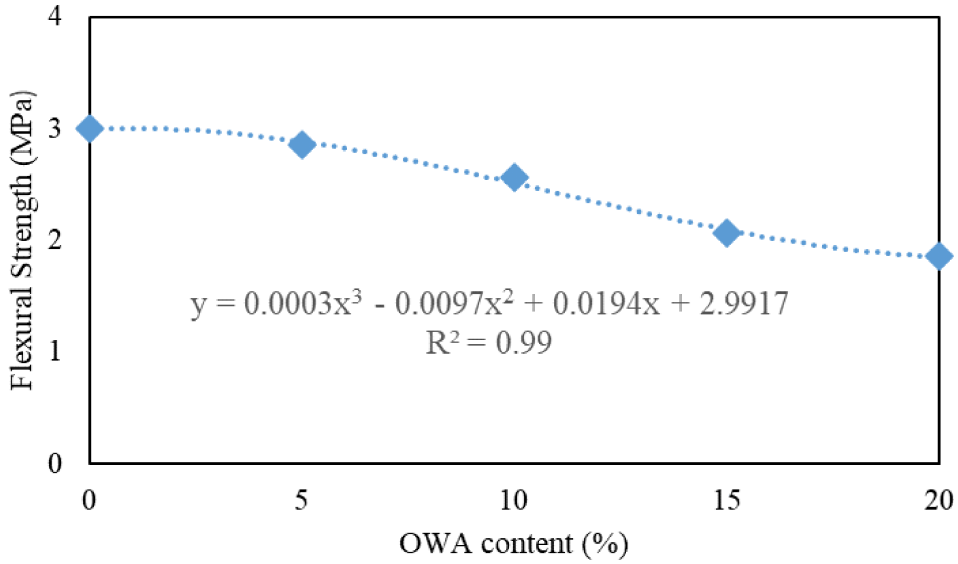

FIGURE 12 | Effect of OWA on the flexural strength of mortar specimens.

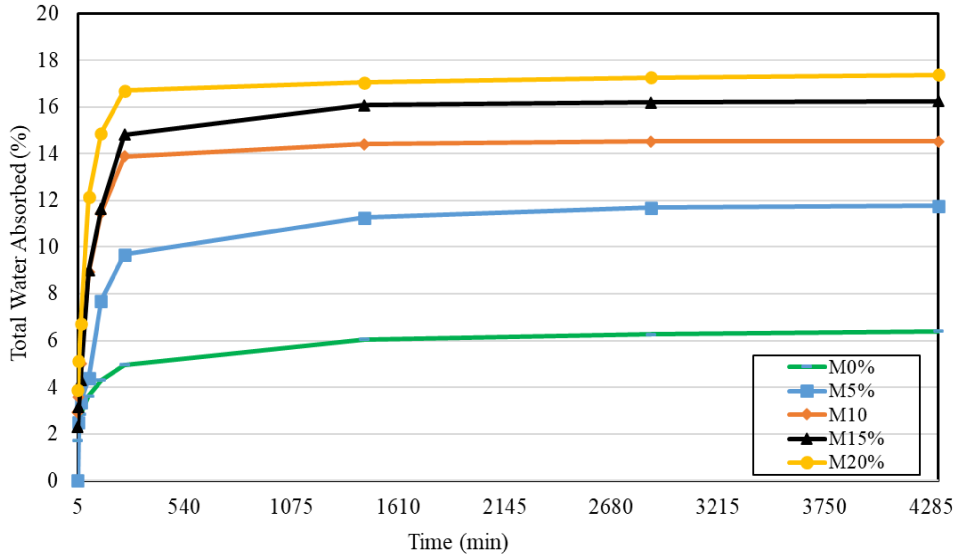

FIGURE 13 | TWA percentages for all mortars at 28 days.

record flexural strengths of 3.3, 3.1, 2.8, 2.3, and 2.1 MPa, respectively. These numerical values reflect percentage decreases of 6%, 14%, 31%, and 38%, respectively. The loss in flexural strength is attributed to the partial substitution of cement with OWA, which increases the number of voids within the matrix and weakens the bond between the OWA and cement paste [58]. By contrast, in examining the impact of wood ash as a substitute for ordinary cement in cementitious systems, an 8% substitution enhanced the 28-day flexural strength by 6% relative to the control concrete [62].

The variation of mortar flexural strength with OWA replacement level was also examined using a cubic regression model, as shown in Figure 12. The resulting best-fit relationship is expressed as: $F(x) = 0.0003x^3 - 0.0097x^2 + 0.019x + 2.992$ with a determination coefficient of $R^2 = 0.99$. The regression indicates a distinct nonlinear trend, where the flexural strength remains nearly unchanged at low OWA contents ($\leq 5\%$) but decreases markedly when the replacement level exceeds 10%.

4.4 | Total Water Absorption (TWA)

Figure 13 depicts the evolution of the TWA percentage at 28 days of curing. As elucidated, all mortar specimens experience a sharp rise in TWA during the early stages (first few hours). Among all the mixtures, the reference mortar indicates a minimum TWA percentage of 6.4%. However, the introduction of OWA negatively affects water ingress, contributing to an increase in TWA as the OWA content rises. After 72 h, the experimental TWA for the mixtures containing 5%, 10%, 15%, and 20% OWA is 11.9%, 14.5%, 16.3%, and 17.4%, respectively, which are equivalent to rises of 86%, 127%, 154%, and 172%. This increase in TWA is attributed to the fact that OWA is a porous body with a lower specific gravity

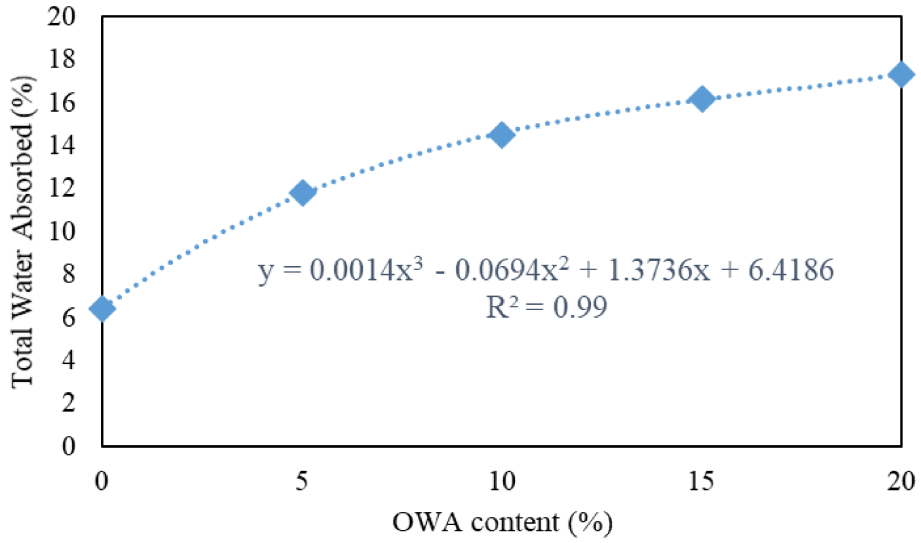

FIGURE 14 | Effect of OWA on TWA of mortar specimens.

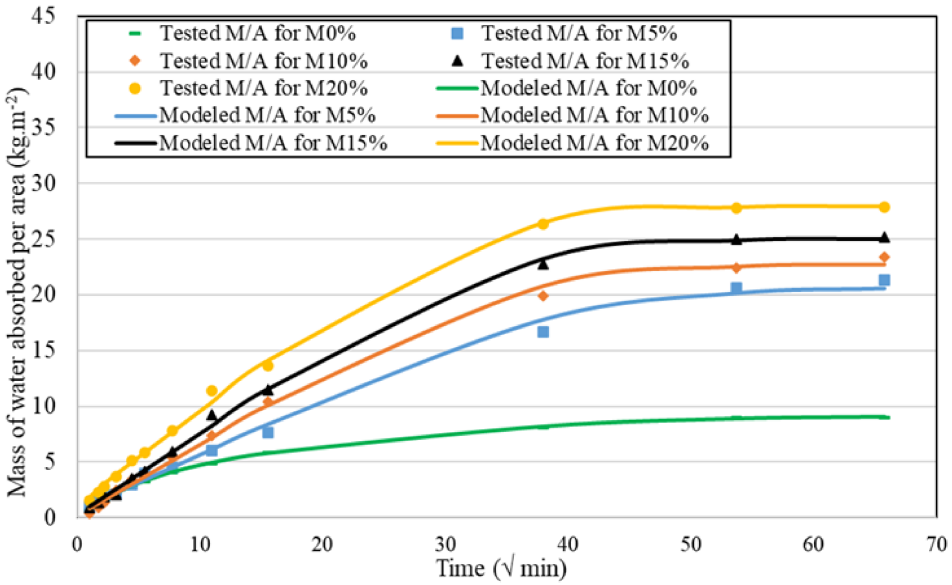

FIGURE 15 | Tested and modeled mass of water absorbed per unit of area at 28 days.

than traditional cement [52]. These physical properties provide mortar with additional voids, which serve as channels for water to penetrate, entailing strong interaction between water and the OWA particles. These two effects interplay to result in higher TWA [64]. Importantly, the considerable augmentation in TWA observed stabilizes during the next 3 days, reflecting that the pores are thoroughly accessed by water, reaching the saturation point and are unable to further absorb more water over the long-term periods [54]. It is worth noting that the observed increase in TWA with higher OWA may have implications for long-term durability. Elevated absorption levels could make these mortars more vulnerable to degradation mechanisms such as freeze–thaw cycling and chloride ingress. Although these durability aspects were not assessed in this study, they should be prioritized in future studies on OWA-based mortars. Compared to OWA-based blended mixtures, bamboo leaf ash revealed a similar water absorption behavior, primarily attributed to the incorporation of additional pores within the specimens [65, 66]. Furthermore, corn cob ash facilitates water transport by 20% at higher replacement levels, accompanied by a 15% decline in density compared to the control mixture [61].

The dependence of total water absorption on OWA replacement level was approximated using a cubic regression model, as illustrated in Figure 14. The fitted equation can be expressed as: $F(x) = 0.0014x^3 - 0.069x^2 + 1.374x + 6.419$ with a high coefficient of determination $R^2 = 0.99$. The regression reveals a clear nonlinear trend, demonstrating that water absorption increases progressively with higher OWA contents, consistent with the rise in material porosity.

4.5 | Capillary Water Absorption (CWA)

Figure 15 illustrates the measured and estimated mass of water absorbed per unit of area over 72 h as a function of the square root

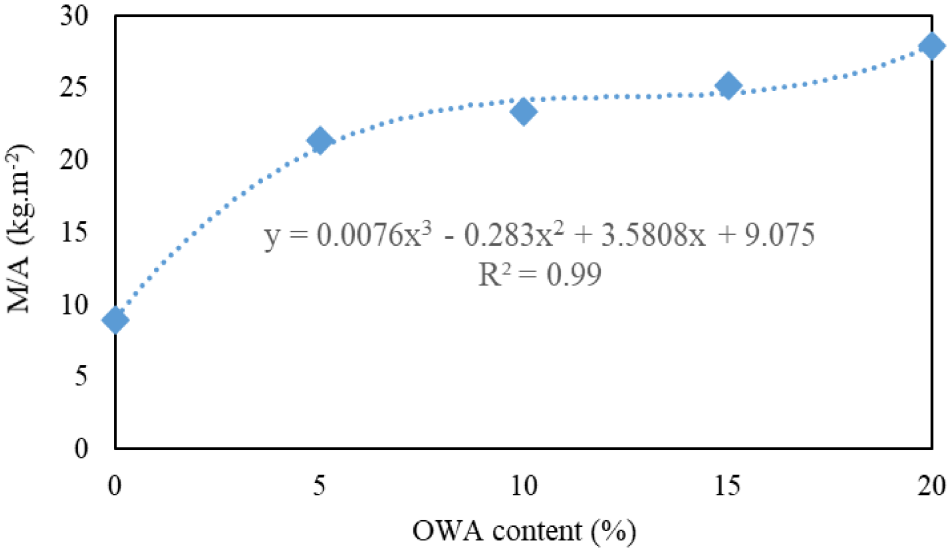

FIGURE 16 | Effect of OWA on the mass of water absorbed per unit area of mortar specimens.

TABLE 4 | Various characteristics determined by the capillary-diffusion model at 28 days.

Mortar	S (kg/m$^2 \cdot s^{1/2}$)	D (m^2/s)	C_0 (kg/m^3)	C (m)
M0%	0.098	6.55×10^{-8}	45.77	0.0045
M5%	0.130	8.10×10^{-8}	199.80	0.0007
M10%	0.180	10.5×10^{-8}	225.21	0.0002
M15%	0.210	11.3×10^{-8}	248.13	0.0003
M20%	0.240	12.6×10^{-8}	265.88	0.0013

of time ($t^{1/2}$) at 28 days. As seen, the CWA consistently increases with increasing OWA content. For instance, the CWA rises from 9 to 28 kg/m^2 as the OWA content increases from 0% to 20%, reaching a peak growth of 211% at 20% OWA. This suggests that incorporating OWA accelerates the water absorption by capillary action, often caused by the increased number of pores within the mortar specimens. The influence of OWA on material porosity has been previously reported in the literature [65]. To describe how capillary water absorption varies with OWA content, a cubic polynomial was fitted to the data (Figure 16). The relationship is: $F(x) = 0.0076x^3 - 0.283x^2 + 3.581x + 9.075$ with a high coefficient of determination $R^2 = 0.99$. The model highlights a clear nonlinear rise in capillary uptake as OWA increases, consistent with greater pore connectivity at higher replacement levels.

The capillary-diffusive model is employed to fit the experimental data and determine the CWA characteristics. This predictive model results in a high degree of correlation (R^2) of 0.99 for all mortars across various replacement levels. Table 4 presents the parameters obtained from the capillary-diffusive model. It appears that S and D follow a similar upward trend, implying that as the OWA levels increase, both S and D also rise consistently. This behavior is highly related to the diffusion mechanism, which allows for the flow of water via the capillary pores, thus demonstrating the strong correlation between those two properties (S and D) [50]. For instance, the reference mortar exhibits the lowest sorptivity and diffusion across all the specimens. After 72 h, the control mixture records S and D measurements of 0.098 kg/m^2. $s^{1/2}$ and 6.5×10^{-8} m^2/s. Nevertheless, these parameters rise with increasing OWA content, reaching peak values of 0.24 kg/m^2. $s^{1/2}$ and 12.6×10^{-8} m^2/s for the mortar with 20% OWA. These growths are equal to 144% and 92% relative to the OWA-free mortar. The porous nature of the OWA is probably a major consequence of this effect, as it introduces more pores into the matrix, therefore promoting water uptake [57]. This indicates that the presence of OWA facilitates water flow through the mortar, either at the surface (via capillary action) or in deeper layers (by diffusion process), producing a matrix that becomes more conductive to rapid water absorption and deep penetration [51–53]. This may increase the susceptibility of OWA-based mortars to long-term deterioration mechanisms such as chloride penetration and moisture-driven damage. Further durability testing is therefore needed to establish the service-life performance of these systems.

4.6 | Chemical Shrinkage

The chemical shrinkage findings throughout 90 days are presented in Figure 17. Notably, the values decrease for mortars with up to 10% OWA, followed by a slight increase in measurements for OWA content beyond this level. At 90 days, the control mortar exhibits a chemical shrinkage value of 620 μm/m. This value ideally drops to 464 μm/m for the samples containing 10% OWA, achieving an ultimate reduction of 25%. As aforementioned, the chemical composition analysis reveals the existence of a considerable concentration of SiO_2, which enables OWA to undergo a pozzolanic reaction [25]. In fact, OWA slowly reacts with calcium hydroxide (CH), a hydration product, thus delaying the early-age hydration mechanism and allowing the mortar to resist the chemical shrinkage [28]. However, once cement replacement by OWA exceeds 10%, chemical shrinkage tends to amplify, achieving a magnitude of 744 μm/m, which reflects an average increase of 20% relative to the reference mortar. The growth in chemical shrinkage at higher replacement levels is attributed to the rise in voids within the matrix, which demands additional water for

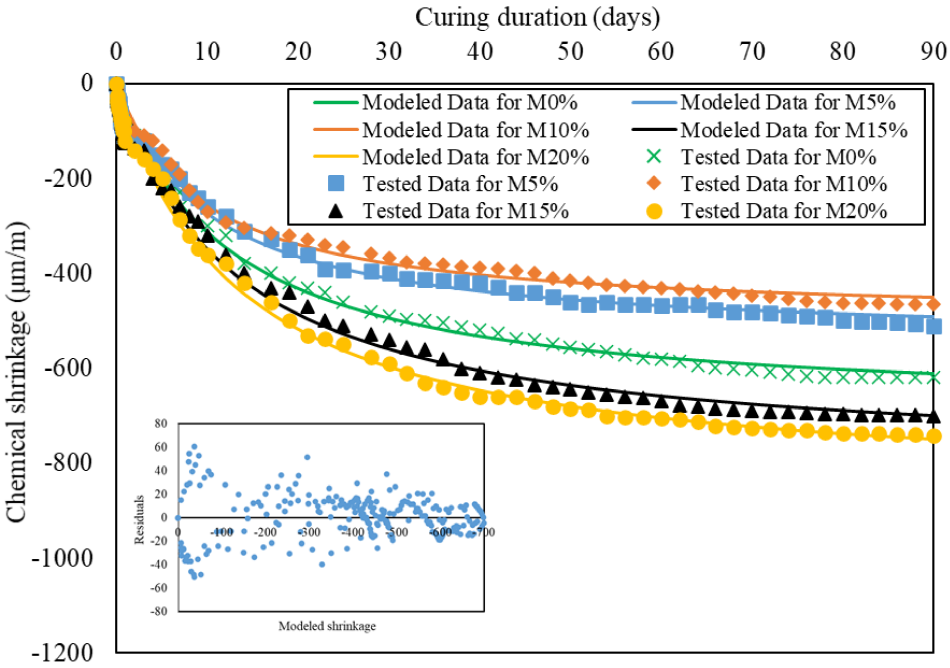

FIGURE 17 | Tested and modeled chemical shrinkage measurements over 90 days.

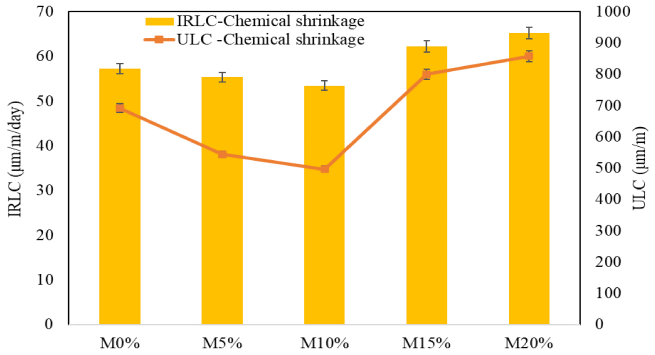

FIGURE 18 | Model outputs for chemical shrinkage measurements (IRLC and ULC).

hydration, thus exacerbating the chemical shrinkage [67]. Comparatively, fly ash—an industrial byproduct from coal combustion in power plants—plays a principal role in controlling the chemical shrinkage mechanism of cementitious systems [68]. Specifically, replacing ordinary cement with 25% fly ash lessened chemical shrinkage by around 20%–30% after 28 days of curing, therefore minimizing the creep risk of the structural body [68]. Literature confirms that combining certain pozzolanic resources, including silica fume, fly ash, and blast furnace slag, can collectively promote the shrinkage-reducing effect, producing a more stable element [69].

The hyperbolic model aids in discerning the chemical shrinkage behavior. The calculated and tested data are perfectly fitted, as evidenced by the great coefficients of determination ($0.92 < R^2 < 0.98$) for multiple OWA percentages. Figure 17 includes an inset residual plot (lower-left) for the hyperbolic fit, showing residuals scattered about the zero line with no systematic curvature. At low modeled shrinkage (30–150 μm/m), the spread is largest, ranging from about −60 to +65 μm/m (typical band ≈ ±45). In the mid-range (200–500 μm/m), dispersion tightens as most residuals fall within −25 to +25 μm/m (typical band ≈ ±15–20). At the far right (600–700 μm/m), variance is smallest; residuals are mostly −20 to +10 μm/m, with a mild negative bias (mean 5–10 μm/m). This fan shape near small shrinkage is consistent with hyperbolic behavior near the asymptote and supports the adequacy of the model fit.

Additionally, the suggested model also determines shrinkage characteristics, including the ultimate length change (ULC) and the initial rate of length change (IRLC) for all mixtures. As illustrated in Figure 18, mortars with up to 10% OWA content indicate a pronounced decline in ULC magnitudes, whereas an increase is found in mortars with higher OWA content. For instance, the ULC value drops from 692 μm/m for M0% to 497 μm/m for M10%, showing a reduction of 28%, while for M20%, the increase stands at 24%. These fluctuations are related to the quantity of water needed for the complete hydration process [58]. Similarly, OWA impacts the IRLC, showing reductions up to 10% OWA, but escalating again at higher replacement levels. More accurately, M10% exhibits a reduction rate of 7%, whereas M20% shows a growth of 12%. This behavior is driven by the fact that early-age chemical shrinkage primarily depends on the hydration mechanism, which is mostly influenced by the incorporation of OWA [67]. It is worth noting that 10% OWA can be appropriate as the optimal percentage, where a substantial minimization of both ULC and IRLC of chemical shrinkage gain is observed.

4.7 | Drying Shrinkage

Figure 19 illustrates the drying shrinkage behavior of all mortars monitored during 90 days. The obtained results indicate fluctuations in drying shrinkage readings. Specifically, incorporating up to 10% OWA reduces drying shrinkage. For instance, the control mixture displays a shrinkage of 1496 μm/m. This value declines

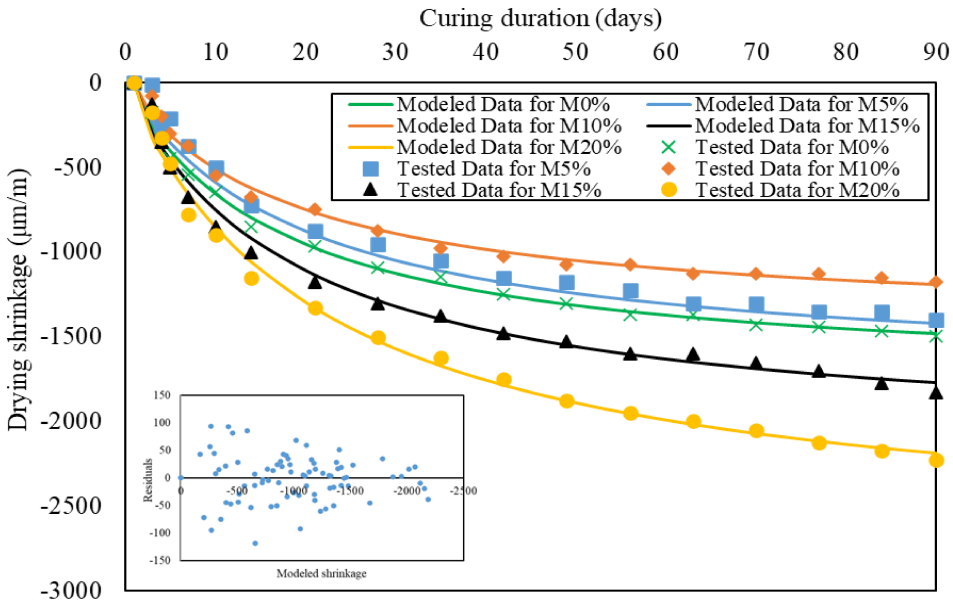

FIGURE 19 | Tested and modeled drying shrinkage measurements over 90 days.

to 1400 and 1175 μm/m for the addition of 5% and 10% OWA, representing decreases of 6% and 21%, respectively. The improvement in drying shrinkage may stem from the pozzolanic reaction of OWA, which efficiently promotes the formation of more C-S-H gel; thus, densifying the matrix. This densification leads to a reduction in the number of voids, diminishing the amount of water available for evaporation upon drying, thus mitigating shrinkage development [70, 71]. However, beyond 10% of OWA addition, particularly at 15% and 20% of replacement, the drying shrinkage rates become higher than those of the reference mortar. The growth in drying shrinkage is mostly related to the excessive replacement of cement with OWA, which contributes to the formation of large and interconnected pore networks. The progressive escape of water reduces the material's stiffness. As a result, the matrix becomes less capable of resisting internal and disjoining stresses between pores, which promotes structural contraction [72].

In comparison, DPA functions as an efficient filler, occupying the pores in the matrix and thereby promoting the shrinkage-reducing effect, achieving a 22% drop after 28 days. This enhancement is associated with reduced moisture loss [73]. The findings of another work justified the substantial impact of RHA on the drying shrinkage performance of concrete at a cement replacement dosage of 20% by weight. At 90 days of curing, drying shrinkage increased by 33% with decreasing RHA particle size [74]. This is mainly attributed to a higher relative humidity, which counteracts the drying shrinkage.

The hyperbolic model shows a strong agreement between experimental and estimated drying shrinkage data. The coefficients of determination (R^2) are 0.985, 0.992, 0.987, 0.985, and 0.994 for mortars M0%, M5%, M10%, M15%, and M20%, respectively. An inset residual plot for the hyperbolic drying-shrinkage fit, with residuals plotted against modeled shrinkage, is presented in Figure 19. The cloud is largely pattern-free and centered near zero. For small magnitudes (≈200–600 μm/m), residuals span about −110 to +120 μm/m (typical band ≈ ±60–70 μm/m). In the mid-range (≈800–1600 μm/m), dispersion tightens to roughly ±40–50 μm/m. At the largest magnitudes (≈1800–2300 μm/m), most points lie within ±25–35 μm/m, with a slight positive bias (mean ≈ +5 to +10 μm/m). This variance tapering with shrinkage magnitude and the absence of curvature indicate that the hyperbolic model captures the drying-shrinkage trend well across the 90-day period.

Figure 20 depicts the ULC and IRLC magnitudes for all mortars. Compared to the control mixture (M0%), the ULC values decrease slightly for 5% and 10% OWA. In contrast, they increase significantly for mixtures with 15% and 20% OWA. Quantitatively, the control mixture records a ULC value of 1760 μm/m, which declines by 2% and 19% for mixtures with 5% and 10% OWA, respectively. The enhancement of long-term drying shrinkage can be linked to the pozzolanic reaction of OWA, which ameliorates the matrix serviceability by lowering drying shrinkage, as explained earlier [49]. Nonetheless, incorporating 15% and 20% of OWA increases the ULC values, attaining 2137 and 2720 μm/m, corresponding to growth of 21% and 55% relative to M0%. This is because of the limited capability of OWA to compensate for the loss of cement amount, which generates additional capillary pores, thus facilitating water loss [75]. High water evaporation within the paste reduces stiffness. As a result, the matrix resists internal pressures less effectively, which amplifies deformation under drying conditions [76]. Moreover, the IRLC generated by the model among all samples at various replacement levels witnesses a consistent pattern with the observed drying shrinkage trend. Hence, the IRLC measurements decrease when OWA is added at levels up to 10%, achieving a drop of 25% for the sample M10%. This effect demonstrates that lower replacement levels improve the resistance to initial drying shrinkage. On the contrary, adding OWA negatively impacts the IRLC, which rises and peaks at 18% for the sample M20%. Based on these trends, it can be concluded that a 10% replacement level is optimal for controlling drying shrinkage.

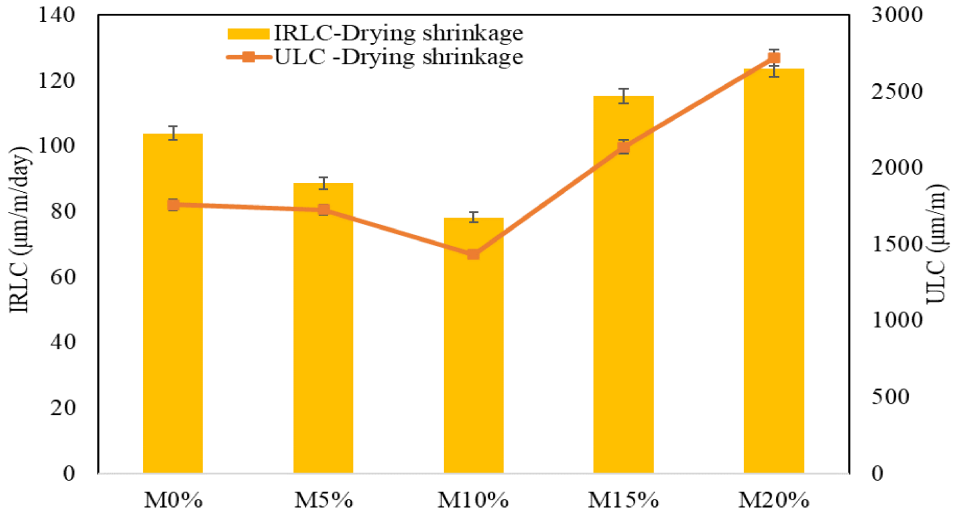

FIGURE 20 | Model outputs for drying shrinkage measurements (IRLC and ULC).

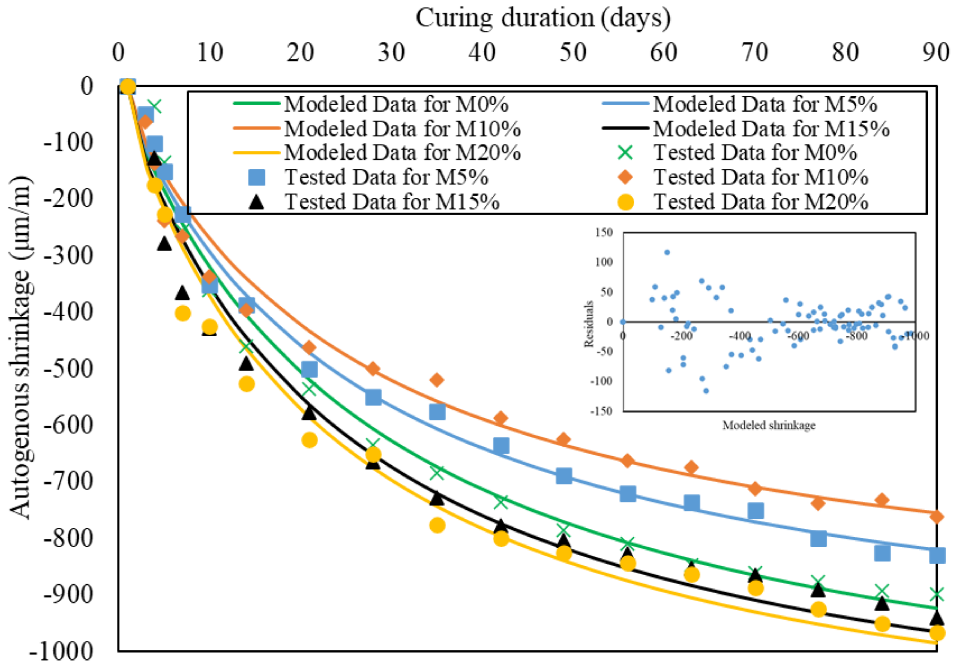

FIGURE 21 | Tested and modeled autogenous shrinkage measurements over 90 days.

4.8 | Autogenous Shrinkage

Figure 21 displays both the calculated and experimental autogenous shrinkage over 90 days. As noticed, lower OWA substitution levels (5% and 10% OWA) desirably enhance the autogenous shrinkage. For instance, the autogenous shrinkage values decrease from 898 to 762 µm/m as the OWA content increases from 0% to 10%, achieving a 15% decrement. The effectiveness of OWA in reducing this type of shrinkage is largely due to the combined effect of the greater C-S-H gel formed and the filler effect of OWA, as it consists of a significant quantity of fine particles filling the voids, making the pores more refined. The interplay between these two factors collectively promotes water retention and internal stress resistance, thus mitigating the development of autogenous shrinkage driven by self-desiccation [17, 19]. Nevertheless, higher replacement percentages (15% and 20% OWA) impair the autogenous shrinkage, intensifying and peaking at 985 µm/m for the sample containing 20% OWA, reflecting an increment of 10%. This intensity is probably linked to the fact that a great quantity of OWA promotes the internal water movement within the mortar, thus augmenting the autogenous shrinkage values. Overall, the implementation of 10% OWA engages the most desirable autogenous shrinkage performance [77, 78]. Similarly, the pozzolanic activity of DPA is essential in mitigating the overall autogenous shrinkage by 35% reported at 90 days. This behavior is achieved through the presence of additional C-S-H gel generated, which withstands internal stresses generated in the cement matrices and produces more stable structures with a lower shrinkage rate [60]. Similarly, RHA diminishes the self-desiccation mechanism due

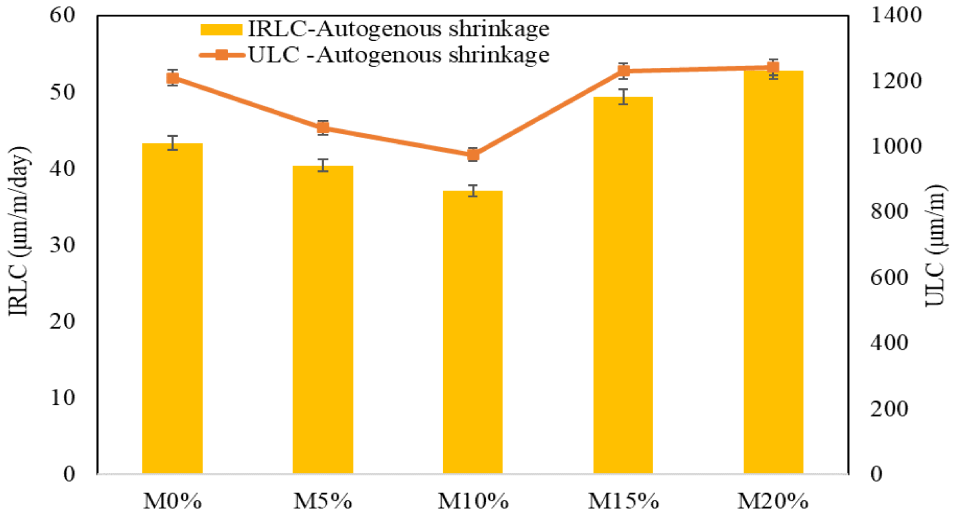

FIGURE 22 | Model outputs for autogenous shrinkage measurements (IRLC and ULC).

to capillary-driven water release. A previous study confirmed that RHA particle size possessed a direct influence on the rate of autogenous shrinkage. As the particle size decreased, the reduction in autogenous shrinkage became less pronounced, varying from 41% to 23% for sizes ranging from 43 to 8.5 µm [79].

In addition, the calculated data strongly agree with the tested data, as confirmed by high coefficients of determination ($R^2 > 0.9$) among all mixtures with OWA varying replacement percentages, ranging from 0% to 20%. Inside Figure 21, the upper-right inset shows the residual plot for the hyperbolic model: points hover around the zero line with no obvious pattern; the scatter is widest at small modeled shrinkage (≈150–300 µm/m, about 90 to +110 µm/m), tightens in the mid-range (≈400–700 µm/m, mostly within ±40–50 µm/m), and is narrowest at the largest magnitudes (≈800–950 µm/m, about ±25–30 µm/m), supporting the adequacy of the fit.

As plotted in Figure 22, the ULC values considerably decrease for samples with 0 to 10% OWA, declining from 1210 to 975 µm/m, corresponding to a reduction rate of 19%. However, a slight rise in ULC is observed when increasing the OWA levels from 15% to 20%. At 90 days, the M20% mixture presents a ULC value of 1242 µm/m, which is equivalent to a modest growth of 3% compared to the OWA-free mortar. A relevant explanation of these fluctuations can be summarized as the long-term autogenous shrinkage pertaining to the remaining moisture available for its evolution [80]. Similarly, OWA substantially improves the IRLC values, highlighting its effect on alleviating initial autogenous shrinkage gain. In particular, adding 10% OWA reduces the initial rate of autogenous shrinkage by 14%. This early-age shrinkage resistance is referred to as the retardation of the hydration mechanism caused by OWA [81]. Actually, OWA particles potentially slow the reaction between OWA and CH, reducing the early hydration; therefore, this limits the progression of self-desiccation of the mortar [70]. Nevertheless, this action is not found in mixtures containing 15% and 20% OWA, where the M20% mixture records a 21% rise. It is worth mentioning that the most favorable reduction in autogenous shrinkage occurs at 10% OWA, which resembles other types of shrinkage.

4.9 | Expansion

The expansion data (both modeled and tested) of all mortars measured during 90 days are illustrated in Figure 23. The observed trend aligns closely with that found in other types of shrinkage. Meanwhile, the inclusion of up to 10% OWA content markedly mitigates the expansion of the mortar specimens, achieving a magnitude of 1038 µm/m, which is equivalent to a 24% drop. This behavior is fundamentally attributable to the pozzolanic activity of OWA, which in turn reacts completely with the hydration product CH, which seems reduced within the matrix. Subsequently, the limited quantity of CH can restrict its reaction with the available expansive compounds in OWA; therefore, withstanding the swelling effect [82]. However, when OWA content exceeds 10% (15% and 20%), the trend reverses. For instance, the samples M15% and M20% exhibit higher values than those for the control mixture. More precisely, the expansion value peaks at 1525 µm/m, corresponding to an augmentation of 12%. When the remaining CH in the matrix is insufficient to react with the excess OWA, other reactions may occur. In particular, reactive components in OWA, such as calcium oxide (CaO), can contribute to expansive reactions, especially the formation of ettringite [83]. A comparable improvement in expansion was also observed with RHA, along with various secondary materials that were introduced into concrete mixtures [79].

The modeled and experimental expansion readings exhibit strong agreement, with a correlation coefficient of 0.99 across all substitution levels, confirming the reliability of the predictive model. Inside Figure 23, the lower-right inset shows the residuals for the hyperbolic expansion fit. They are centered near zero with no obvious curvature: scatter is widest at small modeled expansion (0–300 µm/m, −100 to +40 µm/m), tightens in the mid-range (300–900 µm/m, mostly ±30–40 µm/m), and narrows at the largest values (1000–1500 µm/m, ∼−50 to +20 µm/m) with a slight negative bias (∼−10 µm/m). Overall, the inset supports the adequacy of the model over 90 days.

As observed in Figure 24, the ultimate linear change (ULC) decreases with moderate OWA replacement but increases at

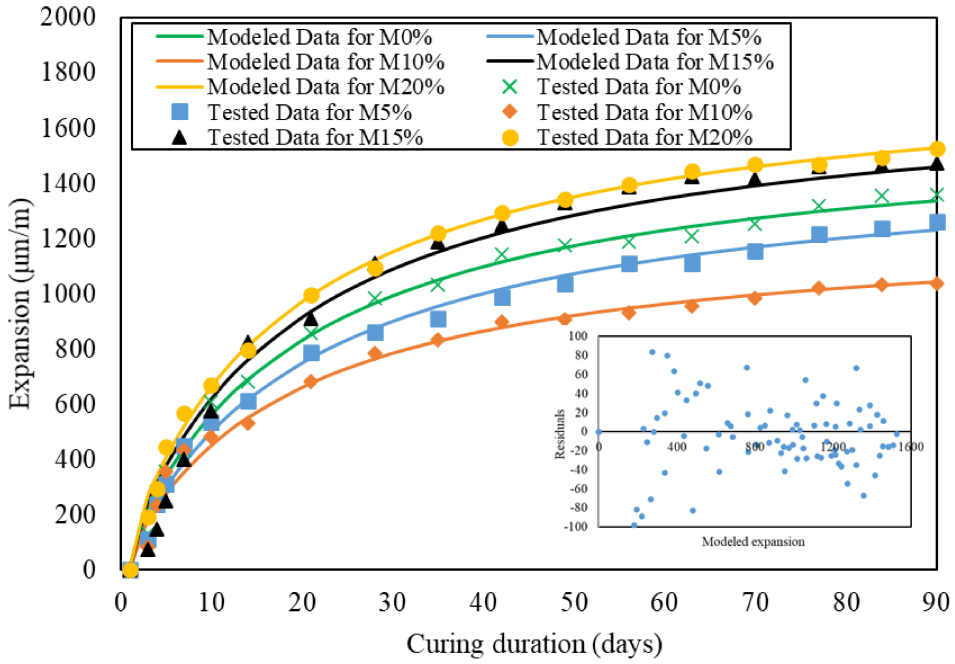

FIGURE 23 | Tested and modeled expansion measurements over 90 days.

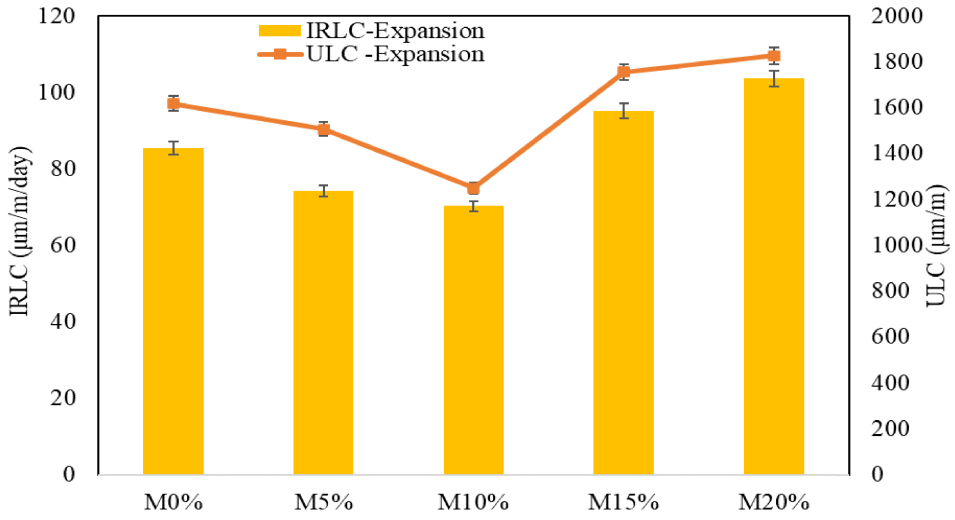

FIGURE 24 | Model outputs for expansion measurements (IRLC and ULC).

higher levels. The control mixture (M0%) records a ULC of 1617 µm/m, which drops to 1490 µm/m (≈8% reduction) at 5% OWA and further to 1249 µm/m (≈23% reduction) at 10% OWA. In contrast, the ULC rises again to 1826 µm/m at 15% OWA and 1875 µm/m at 20% OWA, corresponding to increases of 12% and 16% relative to the control. This nonlinear trend indicates that OWA has a dual effect. At lower replacement levels (≤10%), its pozzolanic reaction consumes calcium hydroxide and contributes to matrix densification, reducing the potential for expansive products. However, at higher OWA dosages, the reduced clinker content and increased porosity create conditions favorable to water ingress and delayed reactions with OWA constituents such as CaO, thereby amplifying expansion [84]. A similar pattern is observed for the IRLC values, which decrease to 18% at 10% OWA (≈25% lower than the control) but subsequently rise, reaching 21% at 20% OWA. This reinforces the interpretation that moderate OWA replacement enhances dimensional stability, whereas higher dosages promote excessive pore connectivity and swelling potential. The early-age increase in expansion remains primarily associated with hydration kinetics, while the long-term behavior reflects the balance between pozzolanic refinement and porosity-driven water uptake [85].

4.10 | Correlations Between Chemical, Drying, Autogenous Shrinkage, and Expansion

Each length change parameter—drying, autogenous, and expansion—correlates with chemical shrinkage as it reflects the internal volume reduction driven by cement hydration during early ages. This volume drop contributes to the development

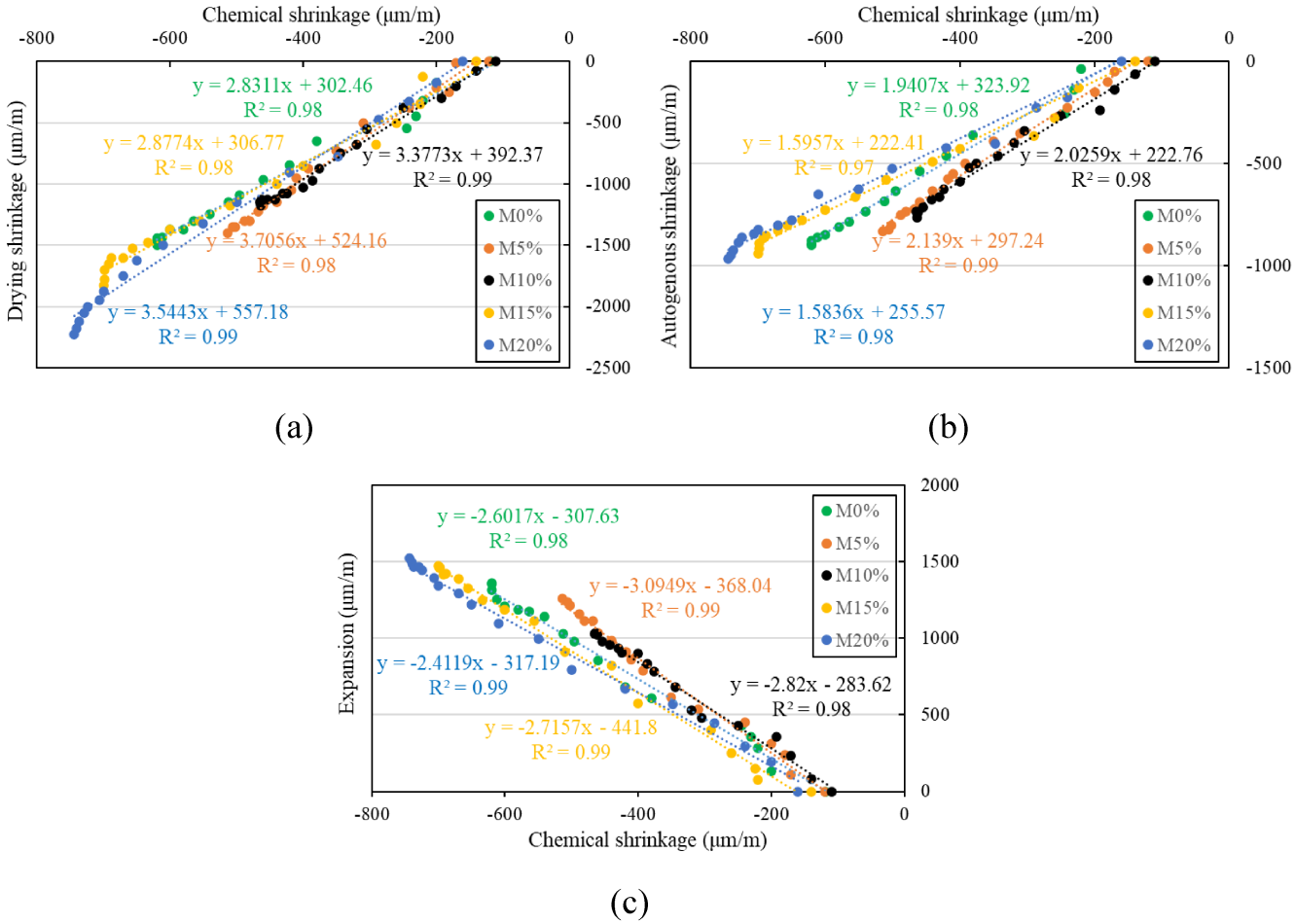

FIGURE 25 | Correlations between: (a) Chemical and drying shrinkage; (b) chemical and autogenous shrinkage; and (c) chemical shrinkage and expansion. *Note:* Model applicability is limited to 0%–20% OWA and 1–90 days.

of capillary tensile stresses in the pore structure, thereby influencing the evolution of other volumetric stability characteristics in the mortar specimens. The regression fits and coefficients of determination are shown in Figure 25 over the curing period. For drying shrinkage, a strong linear relationship with chemical shrinkage is observed, with R^2 values of 0.95, 0.99, 0.95, 0.99, and 0.99 for mixtures M0%, M5%, M10%, M15%, and M20%, respectively. The volume reduction caused by chemical shrinkage enhances internal stresses in the mortar, which increases its tendency to shrink during drying [86]. A likewise positive linear relation exists between autogenous and chemical shrinkage, with high coefficients of determination ($R^2 = 0.99$, 0.99, 0.99, 0.95, and 0.97 for mixtures M0%, M5%, M10%, M15%, and M20%, respectively) reflecting early-age self-desiccation effects [87]. In contrast, expansion is negatively correlated with chemical shrinkage, supported by R^2 values ranging between 0.98 and 0.99. This inverse relationship arises because both phenomena are moisture-dependent: chemical shrinkage results from internal water consumption, whereas expansion is driven by external water ingress [88].

To statistically evaluate these correlations, for each mixture (M0%–M20%) and each pair of volumetric responses, a regression analysis with hypothesis testing is conducted. The hypotheses are defined as follows:

- Null hypothesis (H_0): The first tested property (chemical shrinkage) does not predict other corresponding volumetric response (autogenous, drying, or expansion). In other words, the regression slope is stated as zero.
- Alternative hypothesis (H_1): A linear association exists. The first tested property exhibits an important sensitivity on the second tested property; this is the case when the regression slope is different than zero.

The results (F-test at $\alpha = 0.05$) are presented in Table 5. A p value > 0.05 indicates insufficient evidence of a linear association (i.e., chemical shrinkage does not significantly predict the given shrinkage/expansion response within the studied range). A p value ≤ 0.05 indicates a statistically significant nonzero slope, confirming a linear relationship between chemical shrinkage and the corresponding shrinkage/expansion response. Across all OWA levels, the correlations are statistically significant (all $p \ll 0.05$) for chemical vs. drying shrinkage and chemical vs. autogenous shrinkage, confirming strong positive associations with high R^2 (0.97–0.99). For chemical shrinkage vs. expansion, p values are likewise very small, and the fitted slopes are negative, consistent with the observed inverse trend. Thus, it can be stated that chemical shrinkage serves as a statistically reliable predictor of drying/autogenous shrinkage and expansion.

TABLE 5 | *p* values of volumetric stability correlations across various OWA replacement levels.

Parameter	M0%	M5%	M10%	M15%	M20%
Chemical vs. Drying shrinkage	3.08×10^{-6}	1.16×10^{-9}	1.14×10^{-9}	1.10×10^{-5}	7.69×10^{-9}
Chemical vs. Autogenous shrinkage	6.47×10^{-8}	1.36×10^{-10}	4.58×10^{-8}	4.12×10^{-5}	1.38×10^{-6}
Chemical shrinkage vs. Expansion	4.54×10^{-7}	1.8×10^{-16}	2.22×10^{-7}	3.09×10^{-11}	1.59×10^{-8}

TABLE 6 | ANOVA statistical results at 28 days.

Property	Compressive	Flexural	Chemical	Drying	Autogenous	Expansion
F	8.33	4.52	129.87	100.90	359.52	220.67
p value	0.020	0.066	3.174×10^{-6}	8.208×10^{-6}	6.193×10^{-8}	4.155×10^{-7}

Although the observed correlations are strong, they should not be interpreted as strict causality. Chemical shrinkage is an important parameter influencing volumetric stability, but other mechanisms—such as pore refinement, ITZ behavior, and moisture transport—also contribute. Thus, chemical shrinkage may be regarded as a key indicator of dimensional change tendencies rather than the sole driving factor [46]. It should be mentioned that the regression models presented here are derived exclusively from the present dataset, which may restrict their general applicability. Nevertheless, comparable correlations between chemical shrinkage and other volumetric parameters have also been observed in fiber-reinforced mortars [89, 90], supporting the idea that chemical shrinkage plays a central role in governing volumetric changes across different cementitious systems. Future work should expand chemical shrinkage testing to diverse SCM systems to validate and generalize these correlations, thereby improving their predictive value for engineering applications.

To align with standard practice (28-day reference age in ASTM-based evaluation), a one-way ANOVA ($\alpha = 0.05$) was performed on the 28-day results to assess the effect of OWA replacement level. The outcomes are summarized in Table 6. OWA content significantly affected compressive strength ($p = 0.02$) and all volumetric deformation measures: chemical shrinkage, drying shrinkage, autogenous shrinkage, and expansion, with p values < 0.001 in all cases, indicating clear between-group differences at 28 days. In contrast, the effect on flexural strength at 28 days was not statistically significant ($p = 0.066 > 0.05$), suggesting only a modest sensitivity of flexural strength to OWA within the investigated range.

5 | Conclusions

This study evaluated the influence of OWA as a partial cement substitute (0%–20%) on the physical, mechanical, and volumetric stability properties of mortar, supported by predictive modeling. Based on the findings, the following conclusions are drawn:

- Optimal replacement level: A 10% OWA substitution was identified as the most effective dosage, reducing chemical shrinkage, autogenous shrinkage, drying shrinkage, and expansion by 25%, 15%, 21%, and 24%, respectively, compared to control mortar.
- Mechanical and absorption performance: While compressive and flexural strengths declined with increasing OWA content, the 10% mix maintained compressive strength of 23.5 MPa and flexural strength of 2.8 MPa at 28 days, values that align with benchmarks for non-structural mortars (e.g., ASTM C270 Type $M \geq 17.2$ MPa). At the same level, TWA increased from 6.4% (control) to 14.5% (~127% higher), while CWA rose from 9 to ~18–19 kg/m^2 (~100% higher). These increases reflect higher porosity, which is consistent with trends reported for mortars blended with other SCMs such as fly ash, wood ash, and rice husk ash.
- Predictive modeling: Hyperbolic and capillary-diffusive models successfully captured time-dependent compressive strength and moisture transport, with strong agreement to experimental data ($R^2 > 0.98$). This demonstrates their reliability as predictive tools for OWA-modified mortars.
- Scope and limitations: This study focused on volumetric stability, absorption behavior, and mechanical performance of mortars with $w/c = 0.45$ and 0%–20% OWA. Durability aspects such as sulfate resistance, carbonation, and freeze–thaw behavior were not investigated and should be explored in future research along with microstructural analyses (XRD for phase composition and SEM for particle/matrix morphology and ITZ features) to corroborate pozzolanic activity and elucidate mechanisms underlying the observed trends.

Overall, the results provide both experimental and modeling evidence that controlled incorporation of OWA can improve volumetric stability while maintaining acceptable mechanical performance, supporting its potential as a sustainable supplementary material in mortar production.

Author Contributions

Hassan Ghanem: conceptualization, methodology, formal analysis, investigation, writing – original draft, validation, project administration. **Safa Ghazzawi:** writing – original draft, writing – review and editing, validation, investigation. **Jamal Khatib:** methodology, supervision, writing – review and editing. **Adel Elkordi:** writing – review and editing, supervision, formal analysis, project administration. **Mehmet Serkan Kırgız:** formal analysis, validation, writing – review and editing.

Conflicts of Interest

The authors declare no conflicts of interest.

Data Availability Statement

The data that support the findings of this study are available from the corresponding author upon reasonable request.

References

1. B. Zengin, B. Toydemir, S. Ulukaya, D. Oktay, N. Yüzer, and A. Kocak, "The Effect of Mortar Type and Joint Thickness on Mechanical Properties of Conventional Masonry Walls," *Structural Engineering and Mechanics* 67 (2018): 579–592, https://doi.org/10.12989/sem.2018.67.6.579.

2. H. Basaran, A. Demir, and M. Bagci, "The Behavior of Masonry Walls With Reinforced Plaster Mortar," *Advances in Materials Science and Engineering* 2013 (2013): 436946, https://doi.org/10.1155/2013/436946.

3. C. Wang, J. P. Forth, N. Nikitas, and V. Sarhosis, "Retrofitting of Masonry Walls by Using a Mortar Joint Technique; Experiments and Numerical Validation," *Engineering Structures* 117 (2016): 58–70, https://doi.org/10.1016/j.engstruct.2016.03.001.

4. Y. Sun, Y. Cheng, M. Ding, X. Yuan, and J. Wang, "Research on Properties of High-Performance Cement Mortar for Semiflexible Pavement," *Advances in Materials Science and Engineering* 2018 (2018): 4613074, https://doi.org/10.1155/2018/4613074.

5. S. Rashmi, K. S. Jagadish, and S. Nethravathi, "Stabilized Mud Mortar," *International Journal of Research in Engineering and Technology* 3 (2014): 26–39.

6. V. Corinaldesi, "Environmentally-Friendly Bedding Mortars for Repair of Historical Buildings," *Construction and Building Materials* 35 (2012): 778–784, https://doi.org/10.1016/j.conbuildmat.2012.04.131.

7. M. G. Beltrán, F. Agrela, A. Barbudo, J. Ayuso, and A. Ramirez, "Mechanical and Durability Properties of Concretes Manufactured With Biomass Bottom Ash and Recycled Coarse Aggregates," *Construction and Building Materials* 72 (2014): 231–238, https://doi.org/10.1016/j.conbuildmat.2014.09.019.

8. S. Alkheder, Y. T. Obaidat, and M. Taamneh, "Effect of Olive Waste (Husk) on Behavior of Cement Paste," *Case Studies in Construction Materials* 5 (2016): 19–25, https://doi.org/10.1016/j.cscm.2016.05.001.

9. J. Rosales, M. Cabrera, M. G. Beltrán, M. López, and F. Agrela, "Effects of Treatments on Biomass Bottom Ash Applied to the Manufacture of Cement Mortars," *Journal of Cleaner Production* 154 (2017): 424–435, https://doi.org/10.1016/j.jclepro.2017.04.024.

10. M. Şahmaran, İ. Ö. Yaman, and M. Tokyay, "Transport and Mechanical Properties of Self Consolidating Concrete With High Volume Fly Ash," *Cement and Concrete Composites* 31 (2009): 99–106, https://doi.org/10.1016/j.cemconcomp.2008.12.003.

11. A. Khdair and G. Abu-Rumman, "Sustainable Environmental Management and Valorization Options for Olive Mill Byproducts in the Middle East and North Africa (MENA) Region," *PRO* 8 (2020): 671, https://doi.org/10.3390/pr8060671.

12. M. Cabrera, J. Rosales, J. Ayuso, J. Estaire, and F. Agrela, "Feasibility of Using Olive Biomass Bottom Ash in the Sub-Bases of Roads and Rural Paths," *Construction and Building Materials* 181 (2018): 266–275, https://doi.org/10.1016/j.conbuildmat.2018.06.035.

13. Q. Wang, H. Chu, W. Shi, J. Jiang, and F. Wang, "Feasibility of Preparing Self-Compacting Mortar via Municipal Solid Waste Incineration Bottom Ash: An Experimental Study," *Archives of Civil and Mechanical Engineering* 23, no. 4 (2023): 251, https://doi.org/10.1007/s43452-023-00794-5.

14. Q. Wang, H. Chu, J. Jiang, and B. Zhu, "Enhancing Mechanical Performance and Durability of High Strength Mortar With Incineration Bottom Ash via Al_2O_3 Micro-Powder: An Experimental Study," *Journal of Building Engineering* 89 (2024): 109268, https://doi.org/10.1002/anie.202103557.

15. H. Chu, Q. Wang, and W. Zhang, "Optimizing Ecological Ultra-High Performance Concrete Prepared With Incineration Bottom Ash: Utilization of Al_2O_3 Micro Powder for Improved Mechanical Properties and Durability," *Construction and Building Materials* 426 (2024): 136152, https://doi.org/10.1016/j.conbuildmat.2024.136152.

16. S. Ghazzawi, H. Ghanem, S. Chahal, J. Khatib, and A. Elkordi, "Mechanical and Physical Performance of Cement Paste Containing Olive Waste Ash: Implications for Paving Block Applications," *Applied Sciences* 15 (2025): 3959, https://doi.org/10.3390/app15073959.

17. J. M. Khatib, R. Ramadan, H. Ghanem, A. Elkordi, O. Baalbaki, and M. Kırgız, "Chemical Shrinkage of Paste and Mortar Containing Limestone Fines," *Materials Today: Proceedings* 61 (2022): 530–536, https://doi.org/10.1016/j.matpr.2022.01.288.

18. B. Bissonnette, P. Pierre, and M. Pigeon, "Influence of Key Parameters on Drying Shrinkage of Cementitious Materials," *Cement and Concrete Research* 29 (1999): 1655–1662, https://doi.org/10.1016/S0008-8846(99)00156-8.

19. C. B. Cheah and M. Ramli, "Mechanical Strength, Durability and Drying Shrinkage of Structural Mortar Containing HCWA as Partial Replacement of Cement," *Construction and Building Materials* 30 (2012): 320–329, https://doi.org/10.1016/j.conbuildmat.2011.12.009.

20. K. Ruengsillapanun, T. Udtaranakron, T. Pulngern, W. Tangchirapat, and C. Jaturapitakkul, "Mechanical Properties, Shrinkage, and Heat Evolution of Alkali Activated Fly Ash Concrete," *Construction and Building Materials* 299 (2021): 123954, https://doi.org/10.1016/j.conbuildmat.2021.123954.

21. G. Al-Massri, H. Ghanem, J. Khatib, M. S. Kırgız, and A. Elkordi, "Chemical Shrinkage, Autogenous Shrinkage, Drying Shrinkage, and Expansion Stability of Interfacial Transition Zone Material Using Alkali-Treated Banana Fiber for Concrete," *Journal of Structural Integrity and Maintenance* 9 (2024): 2390650, https://doi.org/10.1080/24705314.2024.2390650.

22. M. Rasoolinejad, S. Rahimi-Aghdam, and Z. P. Bažant, "Prediction of Autogenous Shrinkage in Concrete From Material Composition or Strength Calibrated by a Large Database, as Update to Model B4," *Materials and Structures* 52 (2019): 1–17, https://doi.org/10.1617/s11527-019-1331-3.

23. Q. D. Nguyen, S. Afroz, Y. Zhang, T. Kim, W. Li, and A. Castel, "Autogenous and Total Shrinkage of Limestone Calcined Clay Cement (LC3) Concretes," *Construction and Building Materials* 314 (2022): 125720, https://doi.org/10.1016/j.conbuildmat.2021.125720.

24. J. Khatib, R. Ramadan, H. Ghanem, and A. ElKordi, "Effect of Using Limestone Fines on the Chemical Shrinkage of Pastes and Mortars," *Environmental Science and Pollution Research* 30 (2023): 25287–25298, https://doi.org/10.1007/s11356-022-18496-5.

25. S. Ghazzawi, H. Ghanem, S. El-Zahab, J. Khatib, and A. Elkordi, "Effect of Olive Waste Ash as a Partial Replacement of Cement on Volume Stability of Cement Paste," *Infrastructures* 9 (2024): 193, https://doi.org/10.3390/infrastructures9110193.

26. K. Liu, Z. Shui, T. Sun, G. Ling, X. Li, and S. Cheng, "Effects of Combined Expansive Agents and Supplementary Cementitious Materials on the Mechanical Properties, Shrinkage and Chloride Penetration of Self-Compacting Concrete," *Construction and Building Materials* 211 (2019): 120–129, https://doi.org/10.1016/j.conbuildmat.2019.03.143.

27. T. Zhang, P. Gao, R. Luo, Y. Guo, J. Wei, and Q. Yu, "Measurement of Chemical Shrinkage of Cement Paste: Comparison Study of ASTM C 1608 and an Improved Method," *Construction and Building Materials* 48 (2013): 662–669, https://doi.org/10.1016/j.conbuildmat.2013.07.086.

28. W. Yodsudjai and K. Wang, "Chemical Shrinkage Behavior of Pastes Made With Different Types of Cements," *Construction and Building Materials* 40 (2013): 854–862, https://doi.org/10.1016/j.conbuildmat.2012.11.053.

29. I. Y. Hakeem, I. S. Agwa, B. A. Tayeh, and M. H. Abd-Elrahman, "Effect of Using a Combination of Rice Husk and Olive Waste Ashes on High-Strength Concrete Properties," *Case Studies in Construction Materials* 17 (2022): e01486, https://doi.org/10.1016/j.cscm.2022.e01486.

30. R. Cheraghalizadeh and T. Akcaoglu, "Utilization of Olive Waste Ash and Sea Sand Powder in Self-Compacting Concrete," *Iranian Journal of Science and Technology, Transactions of Civil Engineering* 43 (2019): 663–672, https://doi.org/10.1007/s40996-018-0224-y.

31. M. G. Beltrán, A. Barbudo, F. Agrela, J. R. Jiménez, and J. de Brito, "Mechanical Performance of Bedding Mortars Made With Olive Biomass Bottom Ash," *Construction and Building Materials* 112 (2016): 699–707, https://doi.org/10.1016/j.conbuildmat.2016.02.065.

32. L. Kerrai, S. Belaadi, R. Solimando, and F. R. Zirour, "Valorisation of Organic Waste: Use of Olive Kernels and Pomace for Cement Manufacture," *Journal of Cleaner Production* 277 (2020): 123703, https://doi.org/10.1016/j.jclepro.2020.123703.

33. N. M. Al-Akhras and M. Y. Abdulwahid, "Utilisation of Olive Waste Ash in Mortar Mixes," *Structural Concrete* 11 (2010): 221–228, https://doi.org/10.1680/stco.2010.11.4.221.

34. M. Cruz-Yusta, I. Mármol, J. Morales, and L. Sánchez, "Use of Olive Biomass Fly Ash in the Preparation of Environmentally Friendly Mortars," *Environmental Science & Technology* 45 (2011): 6991–6996, https://doi.org/10.1021/es200968a.

35. C. Wang, Y. Lu, Y. Dai, H. Wu, and Z. Ma, "In-Situ 4D CT Analysis of Microcrack Evolution in Carbonated Fiber-Reinforced Recycled Aggregate Concrete," *Cement and Concrete Composites* 163 (2025): 106161, https://doi.org/10.1016/j.cemconcomp.2025.106161.

36. C. Wang, Z. Du, Y. Zhang, L. Li, and Z. Ma, "Meso-Structural Insights Into Post-Peak Behaviors of Micro Steel Fiber-Reinforced Recycled Aggregate Concrete Using In-Situ 4D CT and DVC Techniques," *Journal of Building Engineering* 100 (2025): 111674, https://doi.org/10.1016/j.jobe.2024.111674.

37. C. Wang, Y. Jiayu, Z. Youchao, W. Huixia, and M. Zhiming, "Advanced In-Situ 4D CT Reconstruction for Exploring Fiber Distribution Effects on the Mechanical Behaviors and Interface Optimization of Carbonated High-Toughness Recycled Aggregate Concrete," *Construction and Building Materials* 473 (2025): 140941, https://doi.org/10.1016/j.conbuildmat.2025.140941.

38. C. Wang, J. Guo, X. Wang, Y. Zhang, and Z. Ma, "Dynamic Mechanical Properties and Damage Constitutive Model of High-Toughness Recycled Aggregate Concrete Under High Strain Rate Impact Loads," *Journal of Building Engineering* 106 (2025): 112589, https://doi.org/10.1016/j.jobe.2025.112589.

39. C. Wang, W. Zhao, Y. Dai, H. Wu, and Z. Ma, "Exploring the Energy Dissipation Mechanism and Toughness Quantitative Model for High-Toughness Recycled Concrete Subjected to Dynamic Impact Loading," *Journal of Building Engineering* 108 (2025): 112809, https://doi.org/10.1016/j.jobe.2025.112809.

40. ASTM C1437, *Standard Test Method for Flow of Hydraulic Cement Mortar* (ASTM International, 2007), 609.

41. ASTM C597, *Standard Test Method for Pulse Velocity Through Concrete* (ASTM International, 2009).

42. ASTM C109/C109M-16a, *Standard Test Method for Compressive Strength of Hydraulic Cement Mortars (Using 2-In. Or [50-Mm] Cube Specimens)* (ASTM International, 2016).

43. ASTM C348-02, *Standard Test Method for Flexural Strength of Hydraulic-Cement Mortars* (ASTM International, 2002).

44. ASTM C1585, *Standard Test Method for Measurement of Rate of Absorption of Water by Hydraulic-Cement Concretes* (ASTM International, 2013).

45. ASTM C1608, *Standard Test Method for Chemical Shrinkage of Hydraulic Cement Paste* (ASTM International, 2007), 667–670.

46. H. Ghanem, R. Ramadan, J. M. Khatib, and A. Elkordi, "A Review on Chemical and Autogenous Shrinkage of Cementitious Systems," *Materials* 17 (2024): 283, https://doi.org/10.3390/ma17020283.

47. L. Barcelo, S. Boivin, P. Acker, J. Toupin, and B. Clavaud, "Early Age Shrinkage of Concrete: Back to Physical Mechanisms," *Concrete Science and Engineering* 3 (2001): 85–91.

48. ASTM C157, *Standard Test Method for Length Change of Hardened Hydraulic-Cement Mortar and Concrete* (ASTM International, 2008).

49. ASTM C192, *Standard Practice for Making and Curing Concrete Test Specimens in the Laboratory* (ASTM International, 2014).

50. L. Yang, D. Gao, Y. Zhang, J. Tang, and Y. Li, "Relationship Between Sorptivity and Capillary Coefficient for Water Absorption of Cement-Based Materials: Theory Analysis and Experiment," *Royal Society Open Science* 6 (2019): 190112, https://doi.org/10.1098/rsos.190112.

51. N. Neithalath, "Evaluating the Short- and Long-Term Moisture Transport Phenomena in Lightweight Aggregate Concretes," *Magazine of Concrete Research* 59 (2007): 435–445, https://doi.org/10.1680/macr.2007.59.6.435.

52. M. Fleury, T. Chevalier, G. Berthe, W. Dridi, and M. Adadji, "Water Diffusion Measurements in Cement Paste, Mortar and Concrete Using a Fast NMR Based Technique," *Construction and Building Materials* 259 (2020): 119843, https://doi.org/10.1016/j.conbuildmat.2020.119843.

53. E. Villar-Cocina, E. Valencia-Morales, J. Vega-Leyva, and J. A. Munoz, "Kinetics of the Water Absorption in GGBS-Concretes: A Capillary-Diffusive Model," *Computers and Concrete* 2 (2005): 19–30, https://doi.org/10.12989/cac.2005.2.1.019.

54. M. Kalid, S. P. Mehrotra, M. Verma, J. Ahmad, and C. Verma, "Performance of Multiblend Cement Under Aggressive Environment," *Indian Concrete Journal* 8 (2002): 22–26.

55. N. S. Martys and C. F. Ferraris, "Capillary Transport in Mortars and Concrete," *Cement and Concrete Research* 27 (1997): 747–760, https://doi.org/10.1016/S0008-8846(97)00052-5.

56. J. C. Tavares, L. F. Lucena, G. F. Henriques, R. L. Ferreira, and M. A. dos Anjos, "Use of Banana Leaf Ash as Partial Replacement of Portland Cement in Eco-Friendly Concretes," *Construction and Building Materials* 346 (2022): 128467, https://doi.org/10.1016/j.conbuildmat.2022.128467.

57. V. M. Sounthararajan and A. Sivakumar, "Ultrasonic Tests on Setting Properties of Cementitious Systems," *ARPN Journal of Engineering and Applied Sciences* 7 (2012): 1424–1435.

58. B. A. Tayeh, M. Hadzima-Nyarko, A. M. Zeyad, and S. Z. Al-Harazin, "Properties and Durability of Concrete With Olive Waste Ash as a Partial Cement Replacement," *Advances in Concrete Construction* 11 (2021): 59–71, https://doi.org/10.12989/acc.2021.11.1.000.

59. H. Ghanem, C. E. Bouz, R. Ramadan, A. Trad, J. Khatib, and A. Elkordi, "Effect of Incorporating Cement and Olive Waste Ash on the Mechanical Properties of Rammed Earth Block," *Infrastructures* 9 (2024): 122, https://doi.org/10.3390/infrastructures9080122.

60. N. I. Blaisi, "Environmental Assessment of Utilizing Date Palm Ash as Partial Replacement of Cement in Mortar," *Journal of Hazardous Materials* 357 (2018): 175–179, https://doi.org/10.1016/j.jhazmat.2018.06.013.

61. G. Fava, T. R. Naik, and M. Pierpaoli, "Compressive Strength and Leaching Behavior of Mortars With Biomass Ash," *Recycling* 3 (2018): 46, https://doi.org/10.3390/recycling3030046.

62. E. E. T. Ercan, L. Andreas, A. Cwirzen, and K. Habermehl-Cwirzen, "Wood Ash as Sustainable Alternative Raw Material for the Production of

Concrete—A Review," *Materials* 16, no. 7 (2023): 2557, https://doi.org/10.3390/ma16072557.

63. ASTM C618-08a, *Standard Specification for Coal Fly Ash and Raw or Calcined Natural Pozzolan for Use in Concrete*. Annual Book of ASTM Standards (ASTM International, 2008).

64. F. Barreca and C. R. Fichera, "Use of Olive Stone as an Additive in Cement Lime Mortar to Improve Thermal Insulation," *Energy and Buildings* 62 (2013): 507–513, https://doi.org/10.1016/j.enbuild.2013.03.040.

65. M. Frías, H. Savastano, E. Villar, M. I. S. de Rojas, and S. Santos, "Characterization and Properties of Blended Cement Matrices Containing Activated Bamboo Leaf Wastes," *Cement and Concrete Composites* 34 (2012): 1019–1023, https://doi.org/10.1016/j.cemconcomp.2012.05.005.

66. A. A. Umoh and I. A. Odesola, "Characteristics of Bamboo Leaf Ash Blended Cement Paste and Mortar," *Civil Engineering Dimension* 17 (2015): 22–28, https://doi.org/10.9744/ced.17.1.22-28.

67. E. Holt, "Contribution of Mixture Design to Chemical and Autogenous Shrinkage of Concrete at Early Ages," *Cement and Concrete Research* 35 (2005): 464–472, https://doi.org/10.1016/j.cemconres.2004.05.009.

68. Y. K. Cho, S. H. Jung, and Y. C. Choi, "Effects of Chemical Composition of Fly Ash on Compressive Strength of Fly Ash Cement Mortar," *Construction and Building Materials* 204 (2019): 255–264, https://doi.org/10.1016/j.conbuildmat.2019.01.208.

69. M. Gesoğlu, E. Güneyisi, and E. Özbay, "Properties of Self-Compacting Concretes Made With Binary, Ternary, and Quaternary Cementitious Blends of Fly Ash, Blast Furnace Slag, and Silica Fume," *Construction and Building Materials* 23, no. 5 (2009): 1847–1854, https://doi.org/10.1016/j.conbuildmat.2008.09.015.

70. K. Bartojay and C. Lucero, *Comparative Analysis on Reducing Concrete Shrinkage and Cracking* (Research and Development Office, US Department of the Interior, Bureau of Reclamation, 2018).

71. H. Ye and A. Radlińska, "A Review and Comparative Study of Existing Shrinkage Prediction Models for Portland and Non-Portland Cementitious Materials," *Advances in Materials Science and Engineering* 2016 (2016): 2418219, https://doi.org/10.1155/2016/2418219.

72. N. M. Al-Akhras, K. M. Al-Akhras, and M. F. Attom, "Performance of Olive Waste Ash Concrete Exposed to Elevated Temperatures," *Fire Safety Journal* 44 (2009): 370–375, https://doi.org/10.1016/j.firesaf.2008.08.006.

73. M. Nasir and W. Al-Kutti, "Performance of Date Palm Ash as a Cementitious Material by Evaluating Strength, Durability, and Characterization," *Buildings* 9, no. 1 (2018): 6, https://doi.org/10.3390/buildings9010006.

74. C. Li, D. Jiang, X. Li, Y. Lv, and K. Wu, "Autogenous Shrinkage and Hydration Property of Cement Pastes Containing Rice Husk Ash," *Case Studies in Construction Materials* 18 (2023): e01943, https://doi.org/10.1016/j.cscm.2023.e01943.

75. F. Beltzung and F. H. Wittmann, "Role of Disjoining Pressure in Cement Based Materials," *Cement and Concrete Research* 35 (2005): 2364–2370, https://doi.org/10.1016/j.cemconres.2005.04.004.

76. L. Wang, S. Zhou, Y. Shi, et al., "The Influence of Fly Ash Dosages on the Permeability, Pore Structure and Fractal Features of Face Slab Concrete," *Fractal and Fractional* 6 (2022): 476, https://doi.org/10.3390/fractalfract6060335.

77. E. Marušić and N. Štirmer, "Autogenous Shrinkage and Expansion Related to Compressive Strength and Concrete Composition," *Journal of Advanced Concrete Technology* 14 (2016): 489–501, https://doi.org/10.3151/jact.14.489.

78. P. Lura, O. M. Jensen, and K. Van Breugel, "Autogenous Shrinkage in High-Performance Cement Paste: An Evaluation of Basic Mechanisms," *Cement and Concrete Research* 33 (2003): 223–232, https://doi.org/10.1016/S0008-8846(02)00890-6.

79. B. A. Tayeh, R. Alyousef, H. Alabduljabbar, and A. Alaskar, "Recycling of Rice Husk Waste for a Sustainable Concrete: A Critical Review," *Journal of Cleaner Production* 312 (2021): 127734, https://doi.org/10.1016/j.jclepro.2021.127734.

80. A. M. Mohamed, B. A. Tayeh, Y. I. A. Aisheh, and M. N. A. Salih, "Utilising Olive-Stone Biomass Ash and Examining Its Effect on Green Concrete: A Review Paper," *Journal of Materials Research and Technology* 24 (2023): 7091–7107, https://doi.org/10.1016/j.jmrt.2023.05.039.

81. L. Barcelo, M. Moranville, and B. Clavaud, "Autogenous Shrinkage of Concrete: A Balance Between Autogenous Swelling and Self-Desiccation," *Cement and Concrete Research* 35 (2005): 177–183, https://doi.org/10.1016/j.cemconres.2004.05.050.

82. C. Lian, Y. Zhuge, and S. Beecham, "The Relationship Between Porosity and Strength for Porous Concrete," *Construction and Building Materials* 25 (2011): 4294–4298, https://doi.org/10.1016/j.conbuildmat.2011.05.005.

83. R. B. Figueira, R. Sousa, L. Coelho, et al., "Alkali-Silica Reaction in Concrete: Mechanisms, Mitigation and Test Methods," *Construction and Building Materials* 222 (2019): 903–931, https://doi.org/10.1016/j.conbuildmat.2019.07.230.

84. T. Achour, E. Jarraya, and N. E. J. I. Jamel, "Apports combinés de l'expérimentation et de la modélisation à la compréhension des propriétés mécaniques des bétons," *Revue des Composites et des Materiaux Avances* 27 (2017): 123–136, https://doi.org/10.3166/rcma.27.123-136.

85. D. Wang, C. Shi, N. Farzadnia, Z. Shi, H. Jia, and Z. Ou, "A Review on Use of Limestone Powder in Cement-Based Materials: Mechanism, Hydration and Microstructures," *Construction and Building Materials* 181 (2018): 659–672, https://doi.org/10.1016/j.conbuildmat.2018.06.075.

86. N. P. Tran, C. Gunasekara, D. W. Law, S. Houshyar, S. Setunge, and A. Cwirzen, "A Critical Review on Drying Shrinkage Mitigation Strategies in Cement-Based Materials," *Journal of Building Engineering* 38 (2021): 102210, https://doi.org/10.1016/j.jobe.2021.102210.

87. D. Sirtoli, M. Wyrzykowski, P. Riva, and P. Lura, "Autogenous and Drying Shrinkage of Mortars Based on Portland and Calcium Sulfoaluminate Cements," *Materials and Structures* 53 (2020): 1–14, https://doi.org/10.1617/s11527-020-01561-1.

88. S. Zhutovsky and K. Kovler, "Chemical Shrinkage of High-Strength/High-Performance Cementitious Materials," *International Review of Civil Engineering* 1 (2010): 110–118, https://doi.org/10.15866/ireche.v10i1.15794.

89. G. Al-Massri, H. Ghanem, J. Khatib, and A. Elkordi, "Influence of Adding Banana Fibers on the Mechanical Properties and Volume Stability of Mortar for Paving Block Applications," *Journal of Natural Fibers* 22, no. 1 (2025): 2464152, https://doi.org/10.1080/15440478.2025.2464152.

90. J. Khatib, R. Ramadan, H. Ghanem, and A. Elkordi, "Effect of Adding Phragmites-Australis Fiber on the Mechanical Properties and Volume Stability of Mortar," *Fibers* 12, no. 2 (2024): 14, https://doi.org/10.1080/15440478.2025.2464152.